

Nonreflecting Boundary Condition for the free Schrödinger equation for hyperrectangular computational domains

Samardhi Yadav¹ and Vishal Vaibhav^{1,2}

¹*Department of Physics, Indian Institute of Technology Delhi, Hauz Khas, New Delhi-110016, India**

²*Optics and Photonics Center, Indian Institute of Technology Delhi, Hauz Khas, New Delhi-110016, India†*

(Dated: August 27, 2024)

In this article, we discuss efficient ways of implementing the transparent boundary condition (TBC) and its various approximations for the free Schrödinger equation on a hyperrectangular computational domain in \mathbb{R}^d with periodic boundary conditions along the $(d-1)$ unbounded directions. In particular, we consider Padé approximant based rational approximation of the exact TBC and a spatially local form of the exact TBC obtained under its high-frequency approximation. For the spatial discretization, we use a Legendre-Galerkin spectral method with a boundary-adapted basis to ensure the bandedness of the resulting linear system. Temporal discretization is then addressed with two one-step methods, namely, the backward-differentiation formula of order 1 (BDF1) and the trapezoidal rule (TR). Finally, several numerical tests are presented to demonstrate the effectiveness of the methods where we study the stability and convergence behaviour empirically.

PACS numbers: 02.30.Ik, 42.81.Dp, 03.65.Nk

NOTATIONS

The set of non-zero positive real numbers (\mathbb{R}) is denoted by \mathbb{R}_+ . For any complex number ζ , $\text{Re}(\zeta)$ and $\text{Im}(\zeta)$ refer to the real and the imaginary parts of ζ , respectively.

I. INTRODUCTION

This article is an extension of the work presented in [1] where we considered the numerical implementation of transparent boundary conditions for the free Schrödinger equation on a rectangular computational domain with periodic boundary condition along one of the unbounded directions. In this work, we consider the elliptic as well as the non-elliptic Schrödinger equation in \mathbb{R}^d , $d = 2, 3$, with periodic boundary condition in $d-1$ dimensions. Both of these models can be encountered in optics [2]. For instance, in the case of a uniform isotropic media, the propagation of optical pulses under slow varying envelope approximation works out to be

$$\left[i \left(\partial_{x_3} + \frac{1}{v_g} \partial_\tau \right) - \frac{1}{2k} \nabla_\perp^2 + \frac{k''}{2} \partial_\tau^2 \right] A(\mathbf{x}, \tau) = 0 \quad (1)$$

where $A(\mathbf{x}, \tau)$ is the envelop, $k = k(\omega_0)$ is the wavenumber corresponding to ω_0 , the central frequency. The quantity $v_g = [k'(\omega_0)]^{-1}$ is the group velocity and $k''(\omega_0)$ is related to group velocity dispersion. Depending on the sign of the coefficients, the equation above can turn out to be elliptic or non-elliptic. Let us emphasize that this work can also be considered as a preparation for treating

more general models which include variable potentials and nonlinearity within the pseudo-differential approach on the lines of [3].

For the purpose of this exposition, we consider the initial value problem (IVP) corresponding to the Schrödinger equation in the following standard form:

$$i\partial_t u + \partial_{x_1}^2 u + \beta \nabla_\perp u = 0, \quad (\mathbf{x}, t) \in \mathbb{R}^d \times \mathbb{R}_+, \quad (2)$$

where $\beta = \pm 1$ and the initial condition $u(\mathbf{x}, 0) = u_0(\mathbf{x})$ is assumed to be compactly supported in the computational domain, Ω_i . We are interested in the efficient numerical solution of (2) on a hyperrectangular computational domain in \mathbb{R}^d with periodic boundary conditions along x_j , $j > 1$.

The primary objective of this work is generalization of the novel Padé approach previously applied to a rectangular domain in our work [4], to a hyperrectangular domain, leveraging its advantages of time-step-independent computational complexity.

The transparent boundary operator for the Schrödinger equation on a hyperrectangular domain has the form $\sqrt{\partial_t - i\Delta_\Gamma}$ where Δ_Γ is the Laplace-Beltrami operator. Note that these operators are nonlocal, both in time as well as space. The earliest numerical implementation for the operator $\sqrt{\partial_t - i\Delta_\Gamma}$ was given by Menza [5] who introduced a Padé approximant based rational approximation for the complex square root function to obtain effectively local boundary conditions. However, this method failed to address the problems arising at the corners of the rectangular domain. In our recent work [4], we reported a novel Padé approach that effectively localizes the transparent boundary operator, offering a computationally efficient solution that handles corners adequately. In this paper, we developed an extension of this approach for the hyperrectangular domain, which reduces the nonlocality in space to solving two-dimensional Schrödinger equations satisfied by certain auxiliary functions on the boundary faces

* Samardhi@physics.iitd.ac.in

† vishal.vaibhav@gmail.com

of the hyperrectangular computational domain, while the temporal nonlocality is handled through rational approximation for $\sqrt{\partial_t}$ operator acting on the auxiliary functions. The novel-Padé method developed in our work ensures that the computational cost and the memory requirement does not grow with increasing time-steps. Furthermore, we provide a detailed comparison of various approximations for the TBCs, including convolution quadrature (CQ) approach, conventional Padé approach (CP), novel Padé approach (NP), and high-frequency approximation. Note that CQ scheme remains nonlocal while others are effectively local.

For the space discretization, we use a Legendre-Galerkin method where a boundary-adapted basis is constructed to ensure the bandedness of the resulting linear system. At the discrete level, the TBCs are formulated as a Robin-type boundary condition at each time-step. In order to homogenize these Robin-type maps needed for the construction of the basis, we also discuss a boundary-lifting process. Temporal discretization is then addressed with two one-step time marching methods, namely, BDF1 and TR. Let us emphasize that an unsuitable temporal discretization of the nonlocal operators may destroy the overall stability of the numerical scheme [6, 7]. To avoid this, we try to match the time-stepping methods in the discretization of the boundary conditions to that of the interior problem.

The paper is organized in the following manner: Sec. II presents the derivation of TBCs followed by a discussion of numerically tractable forms of the TBCs for the 2D problem. This section also discusses the high-frequency approximation of the TBCs. Sec. III presents the derivation of TBCs followed by discussion of novel Padé based representation of TBCs for the 3D problem. In Sec. IV and Sec. VI, we discuss the time-discretization of TBCs and the numerical solution of the IBVP using Legendre-Galerkin method with a boundary-adapted basis for the 2D and 3D problems, respectively. We then confirm the efficiency and stability of our numerical schemes with several numerical tests presented in Sec. V and Sec. VII. Finally, we conclude this paper in Sec. VIII.

II. TBC-2D

Consider a rectangular computational domain with boundary segments parallel to one of the axes (see Fig. 1) with $\Omega_i = (x_l, x_r) \times [-d, d]$ also termed as *interior* domain. By using the decomposition of $u(\mathbf{x}, t) \in \mathcal{L}^2(\mathbb{R} \times [-d, d]) = \mathcal{L}^2(\Omega_i) \oplus \mathcal{L}^2(\Omega_e)$ where $\Omega_e = (\mathbb{R} \times [-d, d]) \setminus \bar{\Omega}_i$ also termed as *exterior* domain. With this in mind, the equivalent formulation of problem (2) in \mathbb{R}^2 can be stated

as

$$\begin{aligned} \text{interior : } & \begin{cases} i\partial_t v + \Delta v = 0, & (\mathbf{x}, t) \in \Omega_i \times \mathbb{R}_+, \\ v(\mathbf{x}, 0) = u_0(\mathbf{x}), & \mathbf{x} \in \Omega_i, \end{cases} \\ \text{exterior : } & \begin{cases} i\partial_t w + \Delta w = 0, & (\mathbf{x}, t) \in \Omega_e \times \mathbb{R}_+, \\ w(\mathbf{x}, 0) = 0, & \mathbf{x} \in \Omega_e, \\ \lim_{|\mathbf{x}_1| \rightarrow \infty} |w(\mathbf{x}, t)| = 0. \end{cases} \end{aligned} \quad (3)$$

$$\text{continuity : } v|_{\Gamma} = w|_{\Gamma}, \quad \partial_n v|_{\Gamma} = \partial_n w|_{\Gamma},$$

where $\Delta = (\partial_{x_1}^2 + \beta \partial_{x_2}^2)$ and Γ denotes the common boundary of the interior and the exterior domains. Also, the initial data is assumed to be compactly supported in Ω_i . For the sake of completeness, we reproduce the results from [1, 3] on the derivation of the TBCs for the system under consideration. Assuming the periodicity behaviour along x_2 , we can express the field $w(x_1, x_2, t)$ in terms of a Fourier series as:

$$\begin{aligned} w(x_1, x_2, t) &= \sum_{m \in \mathbb{Z}} \tilde{w}_m(x_1, t) e^{i\zeta_m x_2}, \\ W(x_1, x_2, z) &= \sum_{m \in \mathbb{Z}} \tilde{W}_m(x_1, z) e^{i\zeta_m x_2}, \end{aligned} \quad (4)$$

where $\tilde{W}_m(x_1, z) = \mathcal{L}_t[\tilde{w}_m(x_1, t)]$ denote the Laplace transform of the field. By employing the Fourier ex-

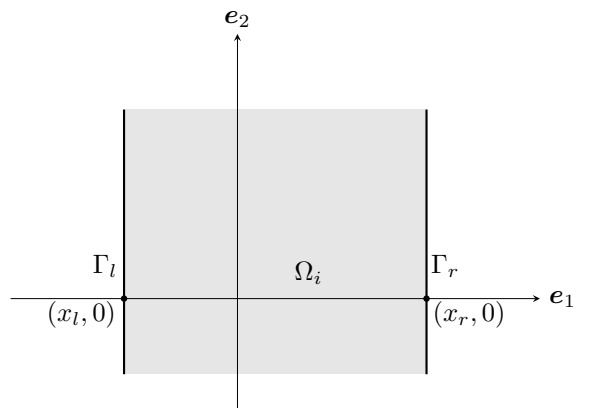


FIG. 1. The figure shows a rectangular domain with periodic boundary conditions along vertical axis.

pansion with respect to x_2 and then taking the Laplace transform of the right exterior problem yields

$$(\partial_{x_1}^2 + \alpha_m^2) \tilde{W}_m(x_1, z) = 0, \quad x_1 \in (x_r, \infty), \quad (5)$$

where $\alpha_m = \sqrt{(iz - \beta \zeta_m^2)}$ such that $\sqrt{\cdot}$ denotes the branch with $\text{Im}(\alpha_m) > 0$. The bounded solution works out to be

$$\partial_{x_1} \tilde{W}_m(x_1, z) = i\alpha_m \tilde{W}_m(x_1, z). \quad (6)$$

To facilitate the inverse Laplace transform, we rewrite the above equation as

$$\mathcal{L}^{-1}[\partial_{x_1} \tilde{W}_m] = \mathcal{L}^{-1}[i\alpha_m^{-1}] \star \mathcal{L}^{-1}[\alpha_m^2 \tilde{W}_m], \quad (7)$$

where ‘ \star ’ represents the convolution operation. In order to carry out the inverse Laplace transformation, let us observe that $\mathcal{L}^{-1}[1/\sqrt{z}](t) = H(t)/\sqrt{\pi t}$ where $H(t)$ denotes the Heaviside step-function. In the following, we use the fractional operators which are denoted by ∂_t^α , $\alpha \in \mathbb{R}$ (see Miller and Ross [8]). For $\alpha < 0$, we obtain the Riemann-Liouville fractional integral of order $|\alpha|$ while $\alpha > 0$ corresponds to fractional derivatives which are introduced as integral order derivatives of fractional integrals. Using the shifting property of Laplace transforms and introducing fractional operators of order $1/2$, we obtain the following result

$$\partial_{x_1} \tilde{w}_m(x_1, t) = e^{i\pi/4} e^{-i\beta\zeta_m^2 t} \partial_t^{-1/2} e^{i\beta\zeta_m^2 t} \times [i\partial_t \tilde{w}_m(x_1, t) - \beta\zeta_m^2 \tilde{w}_m(x_1, t)]. \quad (8)$$

$$\begin{aligned} \partial_{x_1} w(\mathbf{x}, t) &= \frac{e^{i\pi/4}}{\sqrt{\pi}} \int_0^t \int_{\mathbb{R}} [i\partial_\tau w(x_1, x'_2, \tau) + \beta\partial_{x'_2}^2 w(x_1, x'_2, \tau)] \frac{\mathcal{H}(x_2 - x'_2, t - \tau)}{\sqrt{t - \tau}} dx'_2 d\tau \\ &= -(\partial_t - i\beta\partial_{x_2}^2) \frac{e^{-i\pi/4}}{\sqrt{\pi}} \int_0^t \int_{\mathbb{R}} w(x_1, x'_2, \tau) \frac{\mathcal{H}(x_2 - x'_2, t - \tau)}{\sqrt{t - \tau}} dx'_2 d\tau, \end{aligned} \quad (10)$$

where the last step is obtained using the following result from the calculus of fractional operators [8]:

$$\begin{aligned} \partial_t [e^{-i\beta\zeta_m^2 t} \partial_t^{-1/2} e^{i\beta\zeta_m^2 t} \tilde{w}_m(x_1, t)] \\ = e^{-i\beta\zeta_m^2 t} \partial_t^{-1/2} e^{i\beta\zeta_m^2 t} \partial_t \tilde{w}_m(x_1, t). \end{aligned} \quad (11)$$

In order to express the DtN map compactly, we introduce the notation

$$\begin{aligned} (\partial_t - i\beta\partial_{x_2}^2)^{-1/2} f(x_2, t) \\ = \frac{1}{\sqrt{\pi}} \int_0^t \int_{\mathbb{R}} f(x_1, x'_2, \tau) \frac{\mathcal{H}(x_2 - x'_2, t - \tau)}{\sqrt{t - \tau}} dx'_2 d\tau, \end{aligned} \quad (12)$$

so that

$$(\partial_t - i\beta\partial_{x_2}^2)^{1/2} f = (\partial_t - i\beta\partial_{x_2}^2)[(\partial_t - i\beta\partial_{x_2}^2)^{-1/2} f].$$

By using the continuity relations defined in (3), the DtN map on the right segment can be compactly written as

$$\partial_{x_1} v(\mathbf{x}, t) + e^{-i\pi/4} (\partial_t - i\beta\partial_{x_2}^2)^{1/2} v(\mathbf{x}, t) = 0. \quad (13)$$

An equivalent formulation of the IVP (2) on the computational domain $\Omega_i = (x_l, x_r) \times [-d, d]$ with periodic boundary condition along the axis \mathbf{e}_2 is given by

$$\begin{cases} i\partial_t u + (\partial_{x_1}^2 + \beta\partial_{x_2}^2)u = 0, & (\mathbf{x}, t) \in \Omega_i \times \mathbb{R}_+, \\ u(\mathbf{x}, 0) = u_0(\mathbf{x}) \in L^2(\Omega_i), & \text{supp } u_0 \subset \Omega_i; \\ \partial_{n_1} u + e^{-i\pi/4} (\partial_t - i\beta\partial_{x_2}^2)^{1/2} u = 0, & \mathbf{x} \in \Gamma_l \cup \Gamma_r, \\ u(x_1, x_2 + 2d, t) = u(x_1, x_2, t), & t > 0. \end{cases} \quad (14)$$

In order to obtain the inverse Fourier transform of the above relation, let us introduce the kernel which is defined in a distributional sense as

$$\mathcal{H}(x_2, t) = \frac{1}{2d} \sum_{m \in \mathbb{Z}} e^{i(\zeta_m x_2 - \beta\zeta_m^2 t)}. \quad (9)$$

Next by introducing the integral definition for the operator $\partial_t^{-1/2}$ and taking the inverse Fourier transform, the DtN map reads as

Note that the operators present in the DtN maps are non-local in space as well time. For an efficient numerical implementation of this IBVP, we first focus on writing a numerically tractable form of these non-local operators at a continuous level in Sec. II A. We revisit the novel Padé based approach from [4] in Sec. II B which is then contrasted with existing Padé approach for such operators in Sec. II C. Finally, we present an approximate form of these operators under high-frequency approximation from [9] in Sec. II D.

A. Fractional operators based approach

In this section, we explore the possibility of writing the DtN maps in terms of (time-)fractional operators. To achieve this, let us recall the form of the DtN map given by (8) in terms of the Fourier variables so that

$$\begin{aligned} \partial_{x_1} \tilde{w}_m(x_1, t) \\ = e^{i\pi/4} e^{-i\beta\zeta_m^2 t} \partial_t^{-1/2} e^{i\beta\zeta_m^2 t} [i\partial_t - \beta\zeta_m^2] \tilde{w}_m(x_1, t) \\ = i e^{i\pi/4} e^{-i\beta\zeta_m^2 t} \partial_t^{1/2} e^{i\beta\zeta_m^2 t} \tilde{w}_m(x_1, t). \end{aligned} \quad (15)$$

Taking inverse Fourier transform yields

$$\begin{aligned} \partial_{n_1} w &= -e^{i\pi/4} \sum_{m \in \mathbb{Z}} e^{-i\beta\zeta_m^2 t} \partial_t^{1/2} [e^{i\beta\zeta_m^2 t} \tilde{w}_m(x_1, t) e^{i\zeta_m x_2}] \\ &= -e^{i\pi/4} \partial_t^{1/2} \sum_{m \in \mathbb{Z}} [e^{-i\beta\zeta_m^2 (t-t')} \tilde{w}_m(x_1, t') e^{i\zeta_m x_2}] \Big|_{t'=t}. \end{aligned}$$

Introducing the auxiliary function $\varphi(x_1, x_2, \tau_1, \tau_2)$ such that

$$\begin{aligned} & \varphi(x_1, x_2, \tau_1, \tau_2) \\ &= \sum_{m \in \mathbb{Z}} e^{-i\beta\zeta_m^2(\tau_2 - \tau_1)} \tilde{w}_m(x_1, \tau_1) e^{i\zeta_m x_2} \\ &= \sum_{m \in \mathbb{Z}} \left[e^{i\beta\zeta_m^2 \tau_1} \tilde{w}_m(x_1, \tau_1) \right] e^{-i\beta\zeta_m^2 \tau_2 + i\zeta_m x_2}. \end{aligned} \quad (16)$$

The DtN map on segment Γ_r can now be expressed compactly as

$$\partial_{x_1} w(\mathbf{x}, t) = -e^{-i\frac{\pi}{4}} \partial_{\tau_1}^{1/2} \varphi(x_1, x_2, \tau_1, \tau_2) \Big|_{\tau_1, \tau_2=t}. \quad (17)$$

By definition, the numerical implementation of this fractional derivative requires the history of the auxiliary function from the start of the computation which can be facilitated by the IVP satisfied by the auxiliary function:

$$\begin{cases} (\tau_2, x_2) \in (\tau_1, t] \times \mathbb{R} : \\ [i\partial_{\tau_2} + \beta\partial_{x_2}^2] \varphi(x_1, x_2, \tau_1, \tau_2) = 0, \\ \varphi(x_1, x_2 + 2d, \tau_1, \tau_2) = \varphi(x_1, x_2, \tau_1, \tau_2), \\ \varphi(x_1, x_2, \tau_1, \tau_1) = w(x_1, x_2, \tau_1). \end{cases} \quad (18)$$

Note that the history is needed for all $\tau_1 \in [0, t]$ which means that we must solve the IVP for all $\tau_1 \in [0, t]$ over Γ_r . It is interesting to note that the IVP satisfied by the auxiliary function on the segment Γ_r turns out to be a one-dimensional Schrödinger equation. The computation of required history can be understood with the help of the Fig. 2 where we note that the history of the field is needed along the horizontal line up to the diagonal in the (τ_1, τ_2) -plane. The arrows point towards the direction of evolution of the auxiliary function starting from the diagonal values which also serve as the initial conditions.

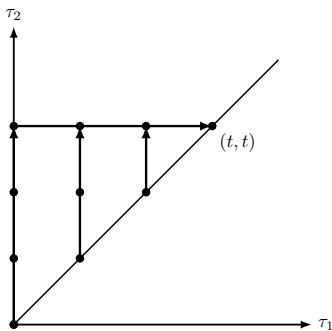


FIG. 2. A schematic is shown in this figure which depicts the evolution of the auxiliary field $\varphi(x_1, x_2, \tau_1, \tau_2)$ in the (τ_1, τ_2) -plane starting from the diagonal which also serves as initial conditions for solving the IVPs (arrow in the line depicts the evolution direction in time). Note that TBCs on $\partial\Omega_i$ require the history of the auxiliary field along the horizontal line up to the diagonal in the (τ_1, τ_2) -plane.

The DtN maps present in (14) in terms of a time-fractional derivative operator reads as

$$\partial_{n_1} u = -e^{-i\frac{\pi}{4}} \partial_{\tau_1}^{1/2} \varphi(x_1, x_2, \tau_1, \tau_2) \Big|_{\tau_1=\tau_2=t}. \quad (19)$$

Here, we would like to mention that fractional operator based approach for the numerical implementation of DtN maps is amenable to convolution quadratures but this approach requires the history from the start of the computation that grows with each time-step making it expensive computationally as well as from a storage point of view.

B. Novel Padé based approach

In this section, we would like to explore the Padé approximant based representation for the 1/2-order temporal derivative in (19) and its other ramifications. This would allow us to obtain an effectively local approximation for the fractional derivative operator. We contrast this with the situation where the history grows with each time-step making it expensive computationally as well as from a storage point of view.

The diagonal Padé approximants for $\sqrt{1-z}$, with negative real axis as the branch-cut, can be used to obtain rational approximation $R_M(z)$ for the function \sqrt{z} as

$$\begin{aligned} R_M(z) &= b_0 - \sum_{k=1}^M \frac{b_k}{z + \eta_k^2}, \\ \text{where } \begin{cases} b_0 = 2M + 1, \\ b_k = \frac{2\eta_k^2(1 + \eta_k^2)}{2M + 1}, \eta_k = \tan \theta_k, \\ \theta_k = \frac{k\pi}{2M + 1}, k = 1, 2, \dots, M. \end{cases} \end{aligned} \quad (20)$$

Here, the expression for the diagonal Padé approximant is taken from [10]. Let us start by introducing a compact notation for the auxiliary functions as:

$$\varphi_{a_1}(x_2, \tau_1, \tau_2) = \varphi(x_{a_1}, x_2, \tau_1, \tau_2), \quad a_1 \in \{l, r\}. \quad (21)$$

Let $z \in \mathbb{C}$, then the Laplace transform of the auxiliary function can be denoted as

$$\mathcal{L}_{\tau_1}[\varphi_{a_1}(x_2, \tau_1, \tau_2)] = \Phi_{a_1}(x_2, z, \tau_2). \quad (22)$$

The DtN maps described in (19) on the segments Γ_{a_1} can be restated as

$$\partial_{x_1} u(\mathbf{x}, t) \pm e^{-i\frac{\pi}{4}} \mathcal{L}_z^{-1} [\sqrt{z} \Phi_{a_1}] \Big|_{\tau_1=\tau_2=t} = 0. \quad (23)$$

Inserting the rational approximation of order M for the function \sqrt{z} as

$$\partial_{x_1} u(\mathbf{x}, t) \pm e^{-i\frac{\pi}{4}} \mathcal{L}_z^{-1} [R_M(z) \Phi_{a_1}] \Big|_{\tau_1=\tau_2=t} \approx 0. \quad (24)$$

The map expressed above is still non-local, however, the rational nature of the expression allows us to obtain an

effectively local approximation for the DtN operation by introducing the auxiliary fields $\varphi_{k,a_1}(x_2, \tau_1, \tau_2)$ at the boundary segment Γ_{a_1} as

$$(z + \eta_k^2)^{-1} \tilde{\Phi}_{a_1}(x_1, x_2, z, \tau_2) = \tilde{\Phi}_{k,a_1}(x_2, z, \tau_2), \quad (25)$$

where $k = 1, 2, \dots, M$. In the physical space, every φ_{k,a_1} satisfy the IVP given by

$$(\partial_{\tau_1} + \eta_k^2) \varphi_{k,a_1}(x_2, \tau_1, \tau_2) = \varphi(x_1, x_2, \tau_1, \tau_2), \quad (26)$$

with the initial conditions set to $\varphi_{k,a_1}(x_2, 0, \tau_2) = 0$. The DtN map now reads as

$$\partial_{x_1} u(\mathbf{x}, t) + e^{-i\frac{\pi}{4}} \left[b_0 u(\mathbf{x}, t) - \sum_{k=1}^M b_k \varphi_{k,a_1}(x_2, t, t) \right] = 0. \quad (27)$$

The solution to the ODEs (26) work out to be

$$\varphi_{k,a_1}(x_2, \tau_1, \tau_2) = \int_0^{\tau_1} e^{-\eta_k^2(\tau_1-s)} \varphi(x_{a_1}, x_2, s, \tau_2) ds. \quad (28)$$

It is easy to verify that the auxiliary fields $\phi_{k,a_1}(x_2, \tau_1, \tau_2)$ satisfy the IVPs given by

$$[i\partial_{\tau_2} + \beta\partial_{x_2}^2] \varphi_{k,a_1}(x_2, \tau_1, \tau_2) = 0. \quad (29)$$

The evolution of the auxiliary fields $\varphi_{k,a_1}(x_2, \tau_1, \tau_2)$ in the (τ_1, τ_2) -plane can be understood with the help of the schematic shown in Fig. 3. The diagonal to diagonal computation of the fields $\varphi_{k,a_1}(x_2, \tau_1, \tau_2)$ consists of first advancing the fields using the IVP established in (29) and then using the ODEs in (26) for the second movement. The novel Padé approach makes the numerical scheme efficient from a storage point of view which is also clear from the schematic presented.

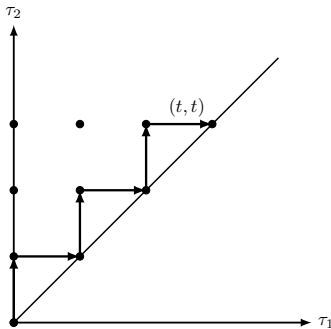


FIG. 3. A schematic depiction of the evolution of the auxiliary fields $\varphi_{k,a_1}(x_2, \tau_1, \tau_2)$ in the (τ_1, τ_2) -plane is provided in this figure.

C. Conventional Padé based approach

In this section, we focus on obtaining an effectively local form for the full operator $(\partial_t - i\beta\partial_{x_2}^2)^{1/2}$ present in

the DtN map in (14) using Padé approximants. One can obtain the rational approximation for the function \sqrt{Z} where $Z = z + i\beta\zeta_m^2$ using (20) now in terms of Z . The DtN map described in (14) on the segments Γ_{a_1} can be restated as

$$\partial_{x_1} u(\mathbf{x}, t) \pm e^{-i\frac{\pi}{4}} \mathcal{F}_{\zeta_m}^{-1} \mathcal{L}_z^{-1} \left[\sqrt{Z} U_m(x_{a_1}, z) \right] = 0. \quad (30)$$

Inserting the rational approximation of order M for the function \sqrt{Z} as

$$\partial_{x_1} u(\mathbf{x}, t) \pm e^{-i\frac{\pi}{4}} \mathcal{F}_{\zeta_m}^{-1} \mathcal{L}_z^{-1} [R_M(Z) U_m] \approx 0. \quad (31)$$

Let $k = 1, 2, \dots, M$, then introducing the auxiliary fields $\{\varphi_k(x_2, t) \leftrightarrow \tilde{\Phi}_{k,m}(z), m \in \mathbb{Z}, z \in \mathbb{C}\}$ at the boundary segments Γ_{a_1} as

$$(z + i\beta\zeta_m^2 + \eta_k^2)^{-1} \tilde{U}_m(x_1, z) = \tilde{\Phi}_{k,m}(z). \quad (32)$$

In the physical space, every φ_k satisfy the IVP given by

$$(i\partial_t + \beta\partial_{x_2}^2 + i\eta_k^2) \varphi_k(x_2, t) = iu(\mathbf{x}, t), \quad (33)$$

with the initial conditions set to $\varphi_k(x_2, 0) = 0$. The DtN map (31) now reads as

$$\partial_{x_1} u(\mathbf{x}, t) \pm e^{-i\pi/4} \left[b_0 u(\mathbf{x}, t) - \sum_{k=1}^M b_k \varphi_k(x_2, t) \right] = 0. \quad (34)$$

D. High-Frequency Approximation

In this section, we focus on obtaining the absorbing boundary conditions for the operator $(\partial_t - i\beta\partial_{x_2}^2)^{1/2}$ under high-frequency approximation. The high-frequency approximation allows us to make the TBCs local with respect to spatial variables. To this end, we consider m -th Fourier component as

$$\mathcal{L}^{-1}[i\alpha_m^{-1}] = \frac{1}{2\pi} \int (iz - \beta\zeta_m^2)^{-1/2} e^{zt} dz. \quad (35)$$

Setting $\xi = zt$, we have

$$\begin{aligned} \mathcal{L}^{-1} \left[\frac{i}{\alpha_m} \right] &= \frac{t^{-\frac{1}{2}}}{2\pi} \int_{a+i\mathbb{R}} \frac{e^\xi}{\sqrt{i\xi - \beta\zeta_m^2 t}} d\xi \\ &= \frac{t^{-\frac{1}{2}}}{2\pi} \int_{a+i\mathbb{R}} \left(1 - \frac{\beta\zeta_m^2 t}{i\xi} \right)^{-\frac{1}{2}} \frac{e^\xi d\xi}{\sqrt{i\xi}} \quad (a > 0) \\ &\sim \frac{t^{-\frac{1}{2}}}{2\pi} \int_{a+i\mathbb{R}} \left(\frac{1}{(i\xi)^{\frac{1}{2}}} + \frac{\beta\zeta_m^2 t}{2(i\xi)^{\frac{3}{2}}} + \frac{3\zeta_m^4 t^2}{8(i\xi)^{\frac{5}{2}}} + \dots \right) e^\xi d\xi \\ &\sim \frac{e^{i\pi/4}}{\Gamma(\frac{1}{2})} t^{-\frac{1}{2}} + \frac{e^{-i\pi/4}}{2\Gamma(\frac{3}{2})} t^{\frac{1}{2}} \beta\zeta_m^2 - \frac{3e^{i\pi/4}}{8\Gamma(\frac{5}{2})} t^{\frac{3}{2}} \beta^2 \zeta_m^4 + \dots \end{aligned}$$

Taking the inverse Fourier transform of (7), we obtain the following form of DtN map as a result of high-frequency approximation on Γ_r :

$$\partial_{x_1} u + e^{-i\frac{\pi}{4}} \partial_t^{\frac{1}{2}} u - \frac{1}{2} e^{i\frac{\pi}{4}} \beta \partial_{x_2}^2 \partial_t^{-\frac{1}{2}} u = 0 \quad \text{mod} \left(\partial_t^{-\frac{3}{2}} \right). \quad (36)$$

III. TBC-3D

In this section, we present an extension of the ideas from \mathbb{R}^2 to \mathbb{R}^3 allowing periodic boundary conditions to be imposed along two of the axes. As it turns out, extension of all the operators defined in Sec. II can be carried out in a natural way.

The initial value problem (IVP) corresponding to the free Schrödinger equation formulated on \mathbb{R}^3 reads as

$$i\partial_t u + (\partial_{x_1}^2 + \beta\partial_{x_2}^2 + \beta\partial_{x_3}^2)u = 0, \quad (\mathbf{x}, t) \in \mathbb{R}^3 \times \mathbb{R}_+, \quad (37)$$

with initial condition $u(\mathbf{x}, 0) = u_0(\mathbf{x})$ which is assumed to be compactly supported in the computational domain, Ω_i . Consider a rectangular cuboidal computational domain with boundary faces parallel to one of the axes (see Fig. 4) with $\Omega_i = (x_l, x_r) \times \mathbb{D}$ where $\mathbb{D} = [-d_2, d_2] \times [-d_3, d_3]$, also termed as *interior* domain. By using the decomposition of $u(\mathbf{x}, t) \in \mathbf{L}^2(\mathbb{R} \times \mathbb{D}) = \mathbf{L}^2(\Omega_i) \oplus \mathbf{L}^2(\Omega_e)$ where $\Omega_e = (\mathbb{R} \times \mathbb{D}) \setminus \bar{\Omega}_i$ also termed as *exterior* domain. With this in mind, the equivalent formulation of problem (37) can be stated as

$$\begin{aligned} \text{interior : } & \begin{cases} i\partial_t v + \Delta v = 0, & (\mathbf{x}, t) \in \Omega_i \times \mathbb{R}_+, \\ v(\mathbf{x}, 0) = u_0(\mathbf{x}), & (\mathbf{x}, t) \in \Omega_i, \end{cases} \\ \text{exterior : } & \begin{cases} i\partial_t w + \Delta w = 0, & (\mathbf{x}, t) \in \Omega_e \times \mathbb{R}_+, \\ w(\mathbf{x}, 0) = 0, & \mathbf{x} \in \Omega_e, \\ \lim_{|x_1| \rightarrow \infty} |w(\mathbf{x}, t)| = 0 \end{cases} \end{aligned} \quad (38)$$

$$\text{continuity : } v|_{\mathbb{F}} = w|_{\mathbb{F}}, \quad \partial_n v|_{\mathbb{F}} = \partial_n w|_{\mathbb{F}},$$

where $\Delta = (\partial_{x_1}^2 + \beta\partial_{x_2}^2 + \beta\partial_{x_3}^2)$ and \mathbb{F} denotes the common regions of the interior and the exterior domains. Also, the initial data is assumed to be compactly supported in Ω_i . Let us introduce the notations

$$\mathbf{x}_\perp = \begin{pmatrix} x_2 \\ x_3 \end{pmatrix} \in \mathbb{D}, \quad \boldsymbol{\zeta}_\perp = \begin{pmatrix} \zeta_2 \\ \zeta_3 \end{pmatrix} \quad (39)$$

where $\boldsymbol{\zeta}_\perp$ denote the covariable corresponding to \mathbf{x}_\perp to be used in the two dimensional Fourier transform. Assuming the periodicity behaviour along \mathbf{e}_2 and \mathbf{e}_3 , we can define the Fourier harmonics as

$$\mathbb{H}_\perp = \left\{ \pi \left(\frac{m_2}{d_2}, \frac{m_3}{d_3} \right)^\top \mid m_2, m_3 \in \mathbb{Z} \right\}. \quad (40)$$

We can express the field $w(x_1, x_2, x_3, t)$ in terms of a Fourier series as

$$\begin{aligned} w(x_1, x_2, x_3, t) &= \sum_{\boldsymbol{\zeta}_\perp \in \mathbb{H}_\perp} \tilde{w}_{\boldsymbol{\zeta}_\perp}(x_1, t) e^{i\boldsymbol{\zeta}_\perp \cdot \mathbf{x}_\perp}, \\ W(x_1, x_2, x_3, z) &= \sum_{\boldsymbol{\zeta}_\perp \in \mathbb{H}_\perp} \widetilde{W}_{\boldsymbol{\zeta}_\perp}(x_1, z) e^{i\boldsymbol{\zeta}_\perp \cdot \mathbf{x}_\perp}, \end{aligned} \quad (41)$$

where $\widetilde{W}_{\boldsymbol{\zeta}_\perp}(x_1, z) = \mathcal{L}_t[\tilde{w}_{\boldsymbol{\zeta}_\perp}(x_1, t)]$ denotes the Laplace transform of the field. Employing the Fourier expansion

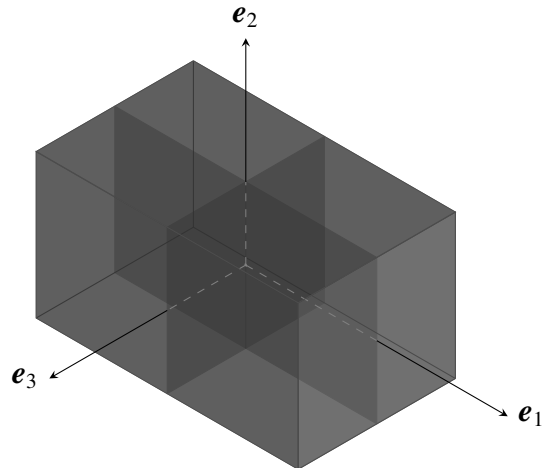


FIG. 4. The figure shows a rectangular cuboidal domain with boundary faces parallel to one of the axes.

with respect to x_2 and x_3 and taking the Laplace transform of the right exterior problem yields

$$(\partial_{x_1}^2 + \alpha^2)\widetilde{W}_{\boldsymbol{\zeta}_\perp}(x_1, z) = 0, \quad x_1 \in (x_r, \infty), \quad (42)$$

where $\alpha = \sqrt{iz - \beta\|\boldsymbol{\zeta}_\perp\|^2} = \sqrt{iz - \beta\zeta_\perp^2}$ such that $\sqrt{\cdot}$ denotes the branch with $\text{Im}(\alpha) > 0$. The boundedness of the solution leads to the relation

$$\partial_{x_1} \widetilde{W}_{\boldsymbol{\zeta}_\perp}(x_1, z) = i\alpha \widetilde{W}(x_1, z). \quad (43)$$

To facilitate the inverse Laplace transform, we rewrite the above equation as

$$\mathcal{L}^{-1}[\partial_{x_1} \widetilde{W}_{\boldsymbol{\zeta}_\perp}] = \mathcal{L}^{-1}[i\alpha^{-1}] \star \mathcal{L}^{-1}[\alpha^2 \widetilde{W}_{\boldsymbol{\zeta}_\perp}], \quad (44)$$

where ‘ \star ’ represents the convolution operation. Using the shifting property of Laplace transforms and introducing fractional operators of order 1/2, we obtain the following result

$$\begin{aligned} \partial_{x_1} \tilde{w}_{\boldsymbol{\zeta}_\perp}(x_1, t) &= e^{i\pi/4} e^{-i\beta\zeta_\perp^2 t} \partial_t^{-1/2} e^{i\beta\zeta_\perp^2 t} \\ & \quad [i\partial_t \tilde{w}_{\boldsymbol{\zeta}_\perp}(x_1, t) - \beta\zeta_\perp^2 \tilde{w}_{\boldsymbol{\zeta}_\perp}(x_1, t)]. \end{aligned} \quad (45)$$

In order to obtain the inverse Fourier transform of the above relation, let us introduce the kernel which is defined in a distributional sense as

$$\mathcal{H}(\mathbf{x}_\perp, t) = \frac{1}{4d_2 d_3} \sum_{\boldsymbol{\zeta}_\perp \in \mathbb{H}_\perp} e^{i(\boldsymbol{\zeta}_\perp \cdot \mathbf{x}_\perp - \beta\zeta_\perp^2 t)}. \quad (46)$$

Next by introducing the integral definition for the operator $\partial_t^{-1/2}$ and taking the inverse Fourier transform, the DtN map reads as

$$\begin{aligned}
\partial_{x_1} w(\mathbf{x}, t) &= \frac{e^{i\pi/4}}{\sqrt{\pi}} \int_0^t \int \int_{\mathbb{R}^2} [i\partial_\tau + \beta\Delta'_\perp] w(x_1, \mathbf{x}'_\perp, \tau) \frac{\mathcal{H}(\mathbf{x}_\perp - \mathbf{x}'_\perp, t - \tau)}{\sqrt{t - \tau}} d^2 \mathbf{x}'_\perp d\tau \\
&= -(\partial_t - i\beta\Delta_\perp) \frac{e^{-i\pi/4}}{\sqrt{\pi}} \int_0^t \int \int_{\mathbb{R}^2} w(x_1, \mathbf{x}'_\perp, \tau) \frac{\mathcal{H}(\mathbf{x}_\perp - \mathbf{x}'_\perp, t - \tau)}{\sqrt{t - \tau}} d^2 \mathbf{x}'_\perp d\tau,
\end{aligned} \tag{47}$$

where the last step is obtained using the following result from the calculus of fractional operators [8]:

$$\partial_t \left[e^{-i\beta\zeta_\perp^2 t} \partial_t^{-1/2} e^{i\beta\zeta_\perp^2 t} \tilde{w}_{\zeta_\perp}(x_1, t) \right] = e^{-i\beta\zeta_\perp^2 t} \partial_t^{-1/2} e^{i\beta\zeta_\perp^2 t} \partial_t \tilde{w}_{\zeta_\perp}(x_1, t). \tag{48}$$

In order to express the DtN map compactly, we introduce the notation

$$(\partial_t - i\beta\Delta_\perp)^{-1/2} f(\mathbf{x}_\perp, t) = \frac{1}{\sqrt{\pi}} \int_0^t \int \int_{\mathbb{R}^2} f(\mathbf{x}'_\perp, \tau) \frac{\mathcal{H}(\mathbf{x}_\perp - \mathbf{x}'_\perp, t - \tau)}{\sqrt{t - \tau}} d^2 \mathbf{x}'_\perp d\tau, \tag{49}$$

so that

$$(\partial_t - i\beta\Delta_\perp)^{1/2} f = (\partial_t - i\beta\Delta_\perp)[(\partial_t - i\beta\Delta_\perp)^{-1/2} f].$$

Using the continuity relations defined in (3), the DtN map on the right segment can be compactly written as

$$\partial_{x_1} v(\mathbf{x}, t) + e^{-i\pi/4} (\partial_t - i\beta\Delta_\perp)^{1/2} v(\mathbf{x}, t) = 0. \tag{50}$$

Set $\mathbf{d}_\perp = (d_2, d_3)^\top$. An equivalent formulation of the IVP (2) on the computational domain $\Omega_i = (x_l, x_r) \times \mathbb{D}$ with periodic boundary condition along the axis \mathbf{e}_2 and \mathbf{e}_3 is given by

$$\begin{cases} i\partial_t u + (\partial_{x_1}^2 + \beta\partial_{x_2}^2 + \beta\partial_{x_3}^2)u = 0, & (\mathbf{x}, t) \in \Omega_i \times \mathbb{R}_+, \\ u(\mathbf{x}, 0) = u_0(\mathbf{x}) \in \mathbf{L}^2(\Omega_i), & \text{supp } u_0 \subset \Omega_i, \\ \partial_n u + e^{-i\pi/4} (\partial_t - i\beta\Delta_\perp)^{1/2} u = 0, & \mathbf{x} \in \mathbb{F}_l \cup \mathbb{F}_r, \\ u(x_1, \mathbf{x}_\perp + 2\mathbf{d}_\perp, t) = u(x_1, \mathbf{x}_\perp, t), & t > 0, \end{cases} \tag{51}$$

where \mathbb{F}_l and \mathbb{F}_r denote the left and right boundary faces of the cuboidal domain, respectively.

A. Fractional operators based approach

In this section, we explore the possibility of writing the DtN maps in terms of (time-)fractional operators. Following the approach presented in Sec. II A, let us recall the form of the DtN map given by (45) in terms of the Fourier variables so that

$$\begin{aligned}
&\partial_{x_1} \tilde{w}_{\zeta_\perp}(x_1, t) \\
&= e^{i\pi/4} e^{-i\beta\zeta_\perp^2 t} \partial_t^{-1/2} e^{i\beta\zeta_\perp^2 t} [i\partial_t - \beta\zeta_\perp^2] \tilde{w}_{\zeta_\perp}(x_1, t) \\
&= i e^{i\pi/4} e^{-i\beta\zeta_\perp^2 t} \partial_t^{1/2} e^{i\beta\zeta_\perp^2 t} \tilde{w}_{\zeta_\perp}(x_1, t)
\end{aligned} \tag{52}$$

Taking inverse Fourier transform yields

$$\begin{aligned}
&\partial_{x_1} w(\mathbf{x}, t) \\
&= -e^{-i\frac{\pi}{4}} \sum_{\zeta_\perp \in \mathbb{H}_\perp} e^{-i\beta\zeta_\perp^2 t} \partial_t^{1/2} \left[e^{i\beta\zeta_\perp^2 t} \tilde{w}_{\zeta_\perp}(x_1, t) e^{i\zeta_\perp \cdot \mathbf{x}_\perp} \right] \\
&= -e^{-i\frac{\pi}{4}} \partial_t^{1/2} \sum_{\zeta_\perp \in \mathbb{H}_\perp} \left[e^{-i\beta\zeta_\perp^2 (t-t')} \tilde{w}_{\zeta_\perp}(x_1, t') e^{i\zeta_\perp \cdot \mathbf{x}_\perp} \right]_{t'=t}.
\end{aligned}$$

Introducing the auxiliary function $\varphi(x_1, \mathbf{x}_\perp, \tau_1, \tau_\perp)$ such that

$$\begin{aligned}
&\varphi(x_1, \mathbf{x}_\perp, \tau_1, \tau_\perp) \\
&= \sum_{\zeta_\perp \in \mathbb{H}_\perp} e^{-i\beta\zeta_\perp^2 (\tau_\perp - \tau_1)} \tilde{w}_{\zeta_\perp}(x_1, \tau_1) e^{i\zeta_\perp \cdot \mathbf{x}_\perp} \\
&= \sum_{\zeta_\perp \in \mathbb{H}_\perp} \left[e^{+i\beta\zeta_\perp^2 \tau_1} \tilde{w}_{\zeta_\perp}(x_1, \tau_1) \right] e^{i(\zeta_\perp \cdot \mathbf{x}_\perp - \beta\zeta_\perp^2 \tau_\perp)}
\end{aligned} \tag{53}$$

The DtN map on the boundary face \mathbb{F}_r can now be expressed compactly as

$$\partial_{x_1} u(\mathbf{x}, t) = -e^{-i\frac{\pi}{4}} \partial_{\tau_1}^{1/2} \varphi(x_1, \mathbf{x}_\perp, \tau_1, \tau_\perp) \Big|_{\tau_1, \tau_\perp = t}. \tag{54}$$

By definition numerical implementation of this fractional derivative requires the history of the auxiliary function from the start of the computation which can be facilitated by the IVP satisfied by the auxiliary function:

$$\begin{cases} (\tau_\perp, \mathbf{x}_\perp) \in (\tau_1, t] \times \mathbb{D} : \\ [i\partial_{\tau_\perp} + \beta\Delta_\perp] \varphi(x_1, \mathbf{x}_\perp, \tau_1, \tau_\perp) = 0; \\ \varphi(x_1, \mathbf{x}_\perp + 2\mathbf{d}_\perp, \tau_1, \tau_\perp) = \varphi(x_1, \mathbf{x}_\perp, \tau_1, \tau_\perp), \\ \varphi(x_1, \mathbf{x}_\perp, \tau_1, \tau_1) = w(x_1, \mathbf{x}_\perp, \tau_1). \end{cases} \tag{55}$$

Note that the history is needed for all $\tau_1 \in [0, t]$ which means that we must solve the IVP for all $\tau_1 \in [0, t]$ over \mathbb{F}_r . It is interesting to note that the IVP satisfied by the auxiliary function on the face \mathbb{F}_r turns out to be a two-dimensional Schrödinger equation. The computation of required history can be understood with the help of the Fig. 5 where we note that the history of the field is needed along the horizontal line up to the diagonal in the (τ_1, τ_\perp) -plane. The arrows point towards the direction of evolution of the auxiliary function starting from the diagonal values which also serve as the initial conditions.

The DtN maps on the boundary faces $\mathbb{F}_l \cup \mathbb{F}_r$ present in (51) in terms of a time-fractional derivative operator reads as

$$\partial_n u = -e^{-i\frac{\pi}{4}} \partial_{\tau_1}^{1/2} \varphi(x_1, \mathbf{x}_\perp, \tau_1, \tau_\perp) \Big|_{\tau_1 = \tau_\perp = t}. \tag{56}$$

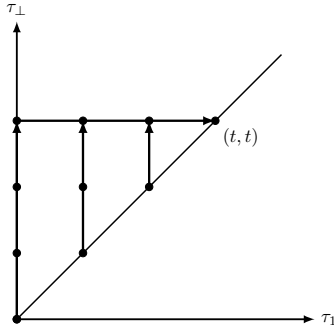


FIG. 5. A schematic is shown in this figure which depicts the evolution of the auxiliary field $\varphi(x_1, \mathbf{x}_\perp, \tau_1, \tau_\perp)$ in the (τ_1, τ_\perp) -plane starting from the diagonal which also serves as initial conditions for solving the IVPs (arrow in the line depicts the evolution direction in time). Note that TBCs on $\partial\Omega_i$ require the history of the auxiliary field along the horizontal line up to the diagonal in the (τ_1, τ_\perp) -plane.

Here, we would like to mention that fractional operator based approach for the numerical implementation of DtN maps is amenable to convolution quadratures but this approach requires the history from the start of the computation that grows with each time-step making it expensive computationally as well as from a storage point of view.

B. Novel Padé based approach

In this section, we would like to explore the Padé approximant based representation for the $1/2$ -order temporal derivative in (56) and its other ramifications. This would allow us to obtain an effectively local approximation for the fractional derivative operator. We contrast this with the situation where the history grows with each time-step making it expensive computationally as well as from a storage point of view. Let us start by introducing a compact notation for the auxiliary functions as:

$$\varphi_{a_1}(\mathbf{x}_\perp, \tau_1, \tau_\perp) = \varphi(x_{a_1}, \mathbf{x}_\perp, \tau_1, \tau_\perp), \quad a_1 \in \{l, r\}. \quad (57)$$

Let $z \in \mathbb{C}$, then the Laplace transform of the auxiliary function can be denoted as

$$\mathcal{L}_{\tau_1}[\varphi_{a_1}(\mathbf{x}_\perp, \tau_1, \tau_\perp)] = \Phi_{a_1}(\mathbf{x}_\perp, z, \tau_\perp). \quad (58)$$

The DtN maps described in (56) on the faces \mathbb{F}_{a_1} can be restated as

$$\partial_{x_1} u(\mathbf{x}, t) \pm e^{-i\pi/4} \mathcal{L}_z^{-1} [\sqrt{z} \Phi_{a_1}] \Big|_{\tau_1=\tau_\perp=t} = 0. \quad (59)$$

Inserting the rational approximation of order M for the function \sqrt{z} as

$$\partial_{x_1} u(\mathbf{x}, t) \pm e^{-i\pi/4} \mathcal{L}_z^{-1} [R_M(z) \Phi_{a_1}] \Big|_{\tau_1=\tau_\perp=t} \approx 0. \quad (60)$$

The map expressed above is still non-local, however, the rational nature of the expression allows us to obtain an

effectively local approximation for the DtN operation by introducing the auxiliary fields $\varphi_{k,a_1}(\mathbf{x}_\perp, \tau_1, \tau_\perp)$ on the boundary faces \mathbb{F}_{a_1} as

$$(z + \eta_k^2)^{-1} \Phi_{a_1}(\mathbf{x}_\perp, z, \tau_\perp) = \Phi_{k,a_1}(\mathbf{x}_\perp, z, \tau_\perp), \quad (61)$$

where $k = 1, 2, \dots, M$. In the physical space, every φ_{k,a_1} satisfy the IVP given by

$$(\partial_{\tau_1} + \eta_k^2) \varphi_{k,a_1}(\mathbf{x}_\perp, \tau_1, \tau_\perp) = \varphi(\mathbf{x}_\perp, \tau_1, \tau_\perp), \quad (62)$$

with the initial conditions set to $\varphi_{k,a_1}(\mathbf{x}_\perp, 0, \tau_\perp) = 0$. The DtN map now reads as

$$\partial_{n_1} u + e^{-i\pi/4} \left[b_0 u(\mathbf{x}, t) - \sum_{k=1}^M b_k \varphi_{k,a_1}(\mathbf{x}_\perp, t, t) \right] = 0. \quad (63)$$

The solution to the ODEs (62) work out to be

$$\varphi_{k,a_1}(\mathbf{x}_\perp, \tau_1, \tau_\perp) = \int_0^{\tau_1} e^{-\eta_k^2(\tau_1-s)} \varphi(x_1, \mathbf{x}_\perp, s, \tau_\perp) ds.$$

It is easy to verify that the auxiliary fields $\varphi_{k,a_1}(\mathbf{x}_\perp, \tau_1, \tau_\perp)$ satisfy the IVPs given by

$$[i\partial_{\tau_\perp} + \beta\Delta_\perp] \varphi_{k,a_1}(\mathbf{x}_\perp, \tau_1, \tau_\perp) = 0. \quad (64)$$

The evolution of the auxiliary fields $\varphi_{k,a_1}(\mathbf{x}_\perp, \tau_1, \tau_\perp)$ in the (τ_1, τ_\perp) -plane can be understood with the help of the schematic shown in Fig. 6. The diagonal to diagonal computation of the fields $\varphi_{k,a_1}(\mathbf{x}_\perp, \tau_1, \tau_\perp)$ consists of first advancing the fields using the IVP established in (64) and then using the ODEs in (62) for the second movement. The novel Padé approach makes the numerical scheme efficient from a storage point of view which is also clear from the schematic presented.

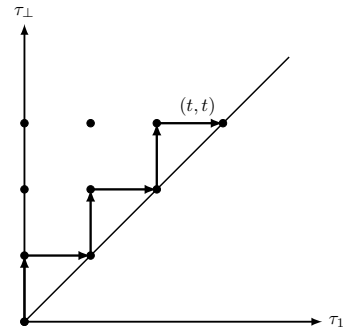


FIG. 6. A schematic depiction of the evolution of the auxiliary fields $\varphi_{k,a_1}(\mathbf{x}_\perp, \tau_1, \tau_\perp)$ in the (τ_1, τ_\perp) -plane is provided in this figure.

IV. NUMERICAL IMPLEMENTATION-2D

In this section, we address the complete numerical solution of the initial boundary-value problem (IBVP)

stated in (14). The formulation of the discrete linear system for the IBVP requires temporal as well as spatial discretization of the problem. To this end, we first discretize the temporal derivative using one-step methods, namely, backward differentiation formula of order 1 (BDF1) and the trapezoidal rule (TR). Subsequently, a compatible temporal discretization scheme is developed for the boundary conditions where we strive to formulate the novel boundary maps at the time-discrete level as a Robin-type boundary condition for each time-step. Finally, for the spatial discretization of the resulting problem, we use a Legendre-Galerkin method where we construct a boundary-adapted basis in terms of the Legendre polynomials followed by a boundary lifting process in order to enforce the boundary conditions exactly.

For the computational domain Ω_i , we introduce a reference domain $\Omega_i^{\text{ref}} = \mathbb{I} \times \pi\mathbb{I}$ keeping in view the typical domain of definition of the orthogonal polynomials being used. In order to describe the associated linear maps between the reference domain and the actual computational domain, we introduce the variables $y_1, y_2 \in \Omega_i^{\text{ref}}$ such that

$$\begin{aligned} x_1 &= J_1 y_1 + \bar{x}_1, & J_1 &= \frac{1}{2}(x_r - x_l), & \bar{x}_1 &= \frac{1}{2}(x_l + x_r), \\ x_2 &= J_2 y_2, & J_2 &= \frac{d}{\pi}, & \beta_1 &= J_1^{-2}, & \beta_2 &= \beta J_2^{-2}. \end{aligned}$$

Let Δt denote the time-step. In the rest of the section, with a slight abuse of notation, we switch to the variables $y_1 \in \mathbb{I}$ and $y_2 \in \pi\mathbb{I}$ for all the discrete approximations of the dependent variables. For instance, $u^j(\mathbf{y})$ is taken to approximate $u(\mathbf{x}, j\Delta t)$ for $j = 0, 1, 2, \dots, N_t - 1$. The temporal discretization of the interior problem using one-step methods is enumerated below:

- The BDF1 based discretization is given by

$$\begin{aligned} i \frac{u^{j+1} - u^j}{\Delta t} + \Delta u^{j+1} &= 0, & \rho &= 1/\Delta t, \\ \implies (\beta_1 \partial_{y_1}^2 + \beta_2 \partial_{y_2}^2) u^{j+1} + i\rho u^{j+1} &= i\rho u^j. \end{aligned} \quad (65)$$

- The TR based discretization is given by

$$\begin{aligned} i \frac{u^{j+1} - u^j}{\Delta t} + \Delta u^{j+1/2} &= 0, & \rho &= 2/\Delta t, \\ \implies (\beta_1 \partial_{y_1}^2 + \beta_2 \partial_{y_2}^2) v^{j+1} + i\rho v^{j+1} &= i\rho u^j, \end{aligned} \quad (66)$$

where we have used the staggered samples of the field defined as

$$v^{j+1} = u^{j+1/2} = \frac{u^{j+1} + u^j}{2}, \quad v^0 = 0. \quad (67)$$

The rest of this section is organized as follows: Sec. IV A addresses the temporal discretization of the boundary maps which is followed by a discussion of the resulting spatial problem in Sec. IV B.

A. Discretizing the boundary conditions

As discussed above, we aim at a compatible temporal discretization of the novel boundary conditions formulated in earlier sections in order to solve the IBVP. To this end, we first discuss the convolution quadrature (CQ) based discretization of the 1/2-order time-fractional derivative present in the TBCs in Sec. II A. Here, we try to match the time-stepping methods in the CQ based discretization of the boundary conditions to that of the interior problem (namely, BDF1 and TR) to preserve the overall stability of the numerical recipe [7]. Next, we discuss the temporal discretization of the boundary maps developed in Sec. II B and Sec. II C using Padé approximants based representation for the fractional operator present in the TBCs. Lastly, we present a CQ based discretization of the fractional derivative operator present in the boundary maps obtained under high-frequency approximation in Sec. II D.

In order to facilitate the temporal discretization of the TBCs, we introduce the equispaced samples of the auxiliary function, $\varphi^{j,k}(y_1, y_2)$, to approximate $\varphi(x_1, x_2, j\Delta t, k\Delta t)$ for $j, k = 0, 1, \dots, N_t - 1$. It follows from the definition of the auxiliary function that the diagonal values of the auxiliary function at the discrete level are determined by the interior field, i.e., $\varphi^{j,j}(y_1, y_2) = u^j(y_1, y_2)$.

Let Δt denote the time-step so that the temporal grid becomes $t_j = j\Delta t$, $j \in \mathbb{N}_0$. The fractional operators $\partial_t^{\pm 1/2}$ can be implemented using the LMM based CQ method. For a given LMM, let the CQ weights be denoted by $\{\omega_k^{(\pm 1/2)} \mid k \in \mathbb{N}_0\}$, then

$$[\partial_t^{\pm 1/2} F_{\pm}]^{j+1} = \rho^{\pm 1/2} F_{\pm}^{j+1} + \rho^{\pm 1/2} \sum_{k=1}^j \omega_{j+1-k}^{(\pm 1/2)} F_{\pm}^k, \quad (68)$$

where ρ is a function of Δt and it is chosen such that $\omega_0^{(\pm 1/2)} = 1$. In the following we restrict ourselves to the trapezoidal rule (TR) and backward differentiation formulae (BDF) of order 1. The recipe for computing the CQ weights for each of the time-stepping methods is enumerated below:

- CQ-BDF1 : The discretization scheme for the time-fractional operators is said to be ‘CQ-BDF1’ if the underlying time-stepping method used in designing the quadrature is BDF1. Let $\nu \in \{+1/2, -1/2\}$ and $\rho = 1/\Delta t$, then the quadrature weights can be computed as follows

$$\omega_k^{(\nu)} = [(k-1-\nu)/k] \omega_{k-1}^{(\nu)}, \quad k \geq 1, \quad (69)$$

where $\omega_0^{(\nu)} = 1$.

- CQ-TR : Let $\rho = 2/\Delta t$, then the quadrature weights for the TR based CQ scheme can be com-

puted as

$$\begin{aligned}\omega_k^{(1/2)} &= (-1)^j \omega_k^{(-1/2)}, \\ \omega_k^{(-1/2)} &= \begin{cases} C_{k/2}, & k \text{ even}, \\ C_{(k-1)/2}, & k \text{ odd}, \end{cases} \quad (70) \\ \text{where } C_n &= \frac{1 \cdot 3 \cdots (2n-1)}{n!2^n}.\end{aligned}$$

The quadrature weights can also be generated using the following recurrence relation [1]:

$$(k+1)\omega_{k+1}^{(\nu)} = (k-1)\omega_{k-1}^{(\nu)} - 2\nu\omega_k^{(\nu)}, \quad k \geq 2, \quad (71)$$

where $\omega_0^{(\nu)} = 1$ and $\omega_1^{(\nu)} = -2\nu$.

1. CQ-BDF1

The discrete scheme for the boundary maps is said to be ‘CQ–BDF1’ if the underlying one-step method in the CQ scheme is BDF1. Let $(\omega_k^{(1/2)})_{k \in \mathbb{N}_0}$ denote the corresponding quadrature weights, then the resulting discretization for the DtN maps described in (19) in terms of $\varphi^{j,k}(y_1, y_2)$ stated as a Robin-type boundary condition reads as

$$\begin{aligned}\partial_{y_1} u^{j+1} \pm \sqrt{\rho/\beta_1} e^{-i\pi/4} u^{j+1} \\ = \mp \sqrt{\rho/\beta_1} e^{-i\pi/4} \mathcal{B} \left[\{\varphi^{k,j+1}(y_{a_1}, y_2)\}_{k=0}^j \right], \quad (72)\end{aligned}$$

where

$$\begin{aligned}\mathcal{B}_{a_1}^{j+1}(y_2) &= \mathcal{B} \left[\{\varphi^{k,j+1}(y_{a_1}, y_2)\}_{k=0}^j \right] \\ &= \sum_{k=1}^{j+1} \omega_k^{(1/2)} \varphi^{j+1-k,j+1}(y_{a_1}, y_2), \quad a_1 \in \{r, l\}.\end{aligned} \quad (73)$$

Set $\alpha_k = \sqrt{\rho/\beta_k} e^{-i\pi/4}$ for $k = 1, 2$. The maps in the compact form reads as

$$\begin{aligned}\partial_{y_1} u^{j+1} - \alpha_1 u^{j+1} &= +\alpha_1 \mathcal{B}_l^{j+1}(y_2), \\ \partial_{y_1} u^{j+1} + \alpha_1 u^{j+1} &= -\alpha_1 \mathcal{B}_r^{j+1}(y_2).\end{aligned} \quad (74)$$

To obtain the history of the field $\varphi(x_1, x_2, \tau_1, \tau_2)$ needed to compute the boundary sums, we employ Fourier Galerkin method (on account of periodicity along x_2) to solve the IVP (18). For the space discretization of the auxiliary equation, we use the Fourier-Galerkin method which employs the series

$$\varphi^{j,k}(y_1, y_2) = \sum_{m \in \mathbb{J}_2} \tilde{\varphi}_m^{j,k}(y_1, y_2) e^{imy_2}, \quad (75)$$

where the index set is given by

$$\mathbb{J}_2 = \left\{ -\frac{N}{2}, \dots, \frac{N}{2} - 1 \right\}. \quad (76)$$

BDF1-based discretization for the IVP in (18) reads as follows:

$$\begin{aligned}i \frac{\tilde{\varphi}_m^{k,j+1} - \tilde{\varphi}_m^{k,j}}{\Delta t} - \beta_2 m^2 \tilde{\varphi}_m^{k,j+1} &= 0, \\ \implies \tilde{\varphi}_m^{k,j+1} &= \frac{\rho}{(\rho + i\beta_2 m^2)} \tilde{\varphi}_m^{k,j}, \quad m \in \mathbb{J}_2.\end{aligned} \quad (77)$$

In terms of $\alpha_2 = \sqrt{\rho/\beta_2} e^{-i\pi/4}$, the coefficients $\tilde{\varphi}_m^{k,j+1}$ satisfy the recurrence relation

$$\tilde{\varphi}_m^{k,j+1} = \frac{\alpha_2^2}{(\alpha_2^2 + m^2)} \tilde{\varphi}_m^{k,j}, \quad (78)$$

with $\tilde{\varphi}_m^{j,j} = \tilde{u}_m^j$.

2. CQ-TR

The discrete scheme is said to be ‘CQ–TR’ if the underlying one-step method in the CQ scheme is TR. Let $(\omega_k^{(1/2)})_{k \in \mathbb{N}_0}$ denote the corresponding quadrature weights, then the resulting discretization scheme for the DtN map described in (19) in terms of $\varphi^{j,k}(y_1, y_2)$ stated as a Robin-type boundary condition (consistent with staggered samples of interior field) reads as

$$\begin{aligned}\partial_{y_1} v^{j+1} \pm \alpha_1 v^{j+1} \\ = \mp \frac{1}{2} \alpha_1 \left(\mathcal{B} \left[\{\varphi_{a_1}^{k,j+1}\}_{k=0}^j \right] + \mathcal{B} \left[\{\varphi_{a_1}^{k,j}\}_{k=0}^{j-1} \right] \right), \quad (79)\end{aligned}$$

where the history operator \mathcal{B} is defined in the similar manner as in the case of BDF1 except the quadrature weights. Let $\mathcal{B}^{j+1/2} = (\mathcal{B}^{j+1} + \mathcal{B}^j)/2$, then the maps can be compactly written as

$$\begin{aligned}\partial_{y_1} v^{j+1} - \alpha_1 v^{j+1} &= +\alpha_1 \mathcal{B}_l^{j+1/2}(y_2), \\ \partial_{y_1} v^{j+1} + \alpha_1 v^{j+1} &= -\alpha_1 \mathcal{B}_r^{j+1/2}(y_2).\end{aligned} \quad (80)$$

Once again, we solve the IVP for the auxiliary function in similar manner as that of BDF1 except using TR-based discretization of the IVP (18) which reads as follows:

$$\begin{aligned}i \left(\frac{\tilde{\varphi}_m^{k,j+1} - \tilde{\varphi}_m^{k,j}}{\Delta t} \right) - \beta_2 m^2 \left(\frac{\tilde{\varphi}_m^{k,j+1} + \tilde{\varphi}_m^{k,j}}{2} \right) &= 0, \\ \implies \tilde{\varphi}_m^{k,j+1} &= \left(\frac{\rho - i\beta_2 m^2}{\rho + i\beta_2 m^2} \right) \tilde{\varphi}_m^{k,j}.\end{aligned} \quad (81)$$

In terms of $\alpha_2 = \sqrt{\rho/\beta_2} e^{-i\pi/4}$, the coefficients $\tilde{\varphi}_m^{j,k}$ satisfy the recurrence relation

$$\tilde{\varphi}_m^{k,j+1} = \left(\frac{\alpha_2^2 - m^2}{\alpha_2^2 + m^2} \right) \tilde{\varphi}_m^{k,j}. \quad (82)$$

3. NP-BDF1

The discrete scheme for the boundary maps is said to be ‘NP–BDF1’ if the temporal derivatives in the realization of the boundary maps, dubbed as ‘NP’, developed

in Sec. II B are discretized using the one-step method BDF1. To achieve this, we start by writing the time-discrete form of the DtN maps present in (27) in the reference domain as

$$\sqrt{\beta_1} \partial_{y_1} \tilde{u}_m^{j+1} \pm e^{-i\pi/4} \left[b_0 \tilde{u}_m^{j+1} - \sum_{k=1}^M b_k \tilde{\varphi}_{k,m}^{j+1,j+1} \right] = 0. \quad (83)$$

In order to turn these equations into a Robin-type boundary condition, we need to compute the discrete samples $\tilde{\varphi}_{k,m}^{j+1,j+1}$ by considering the ODEs established for these auxiliary function earlier. Here, we discuss the BDF1-based discretization of (26) by first employing Fourier expansion: Setting $\rho = 1/\Delta t$ and for $k = 1, 2, \dots, M$, we have

$$\begin{aligned} \frac{\tilde{\varphi}_{k,m}^{j+1,j+1} - \tilde{\varphi}_{k,m}^{j,j+1}}{\Delta t} + \eta_k^2 \tilde{\varphi}_{k,m}^{j+1,j+1} &= \tilde{\varphi}_m^{j+1,j+1} \\ \implies \tilde{\varphi}_{k,m}^{j+1,j+1} &= \frac{\rho}{(\rho + \eta_k^2)} \tilde{\varphi}_{k,m}^{j,j+1} + \frac{1}{(\rho + \eta_k^2)} \tilde{u}_m^{j+1}. \end{aligned} \quad (84)$$

Introduce the scaling $\bar{\eta}_k = \eta_k/\sqrt{\rho}$ so that

$$\tilde{\varphi}_{k,m}^{j+1,j+1} = \frac{1}{(1 + \bar{\eta}_k^2)} \left[\tilde{\varphi}_{k,m}^{j,j+1} + \frac{1}{\rho} \tilde{u}_m^{j+1} \right]. \quad (85)$$

The value of $\tilde{\varphi}_{k,m}^{j,j+1}$ can be obtained by propagation along τ_2 using $\tilde{\varphi}_{k,m}^{j,j}$ as the initial condition:

$$\tilde{\varphi}_{k,m}^{j,j+1} = \frac{1}{(1 + \alpha_2^{-2} m^2)} \tilde{\varphi}_{k,m}^{j,j}, \quad m \in \mathbb{J}_2. \quad (86)$$

Next we plug-in the value of $\tilde{\varphi}_{k,m}^{j+1,j+1}$ in (83) to obtain

$$\begin{aligned} \partial_{y_1} \tilde{u}_m^{j+1} \pm \alpha_1 \varpi \tilde{u}_m^{j+1} \\ = \mp \frac{\alpha_1}{(1 + \alpha_2^{-2} m^2)} \left[\sum_{k=1}^M \Gamma_k \tilde{\varphi}_{k,m}^{j,j} \right] = \mp \alpha_1 \tilde{\mathcal{B}}_{m,a_1}^{j+1}, \end{aligned} \quad (87)$$

where we have set $\bar{b}_0 = b_0/\sqrt{\rho}$, $\bar{b}_k = b_k/\sqrt{\rho}$ and

$$\varpi = \bar{b}_0 + \frac{1}{\rho} \sum_{k=1}^M \Gamma_k, \quad \Gamma_k = -\bar{b}_k/(1 + \bar{\eta}_k^2). \quad (88)$$

Note that these Robin type maps are written for each component in the Fourier series. Also observe that ϖ is independent of m in this case which allows us to take inverse Fourier transform of these maps and obtain the form of maps in the physical space as follows:

$$\partial_{y_1} u^{j+1} \pm \alpha_1 \varpi u^{j+1} = \mp \alpha_1 \mathcal{B}_{a_1}^{j+1}, \quad (89)$$

where

$$\mathcal{B}_{a_1}^{j+1}(y_2) = \sum_{m \in \mathbb{J}_2} \tilde{\mathcal{B}}_{m,a_1}^{j+1} e^{im y_2}, \quad a_1 \in \{r, l\}. \quad (90)$$

4. NP-TR

The discrete scheme for the boundary maps is said to be ‘NP-TR’ if the temporal derivatives in the realization of the boundary maps, dubbed as ‘NP’, developed in Sec. II B are discretized using the one-step method TR. To achieve this, we start by writing the time-discrete form of the DtN maps present in (27) in the reference domain as

$$\sqrt{\beta_1} \partial_{y_1} \tilde{v}_m^{j+1} \pm e^{-i\pi/4} \left[b_0 \tilde{v}_m^{j+1} - \sum_{k=1}^M b_k \tilde{\varphi}_{k,m}^{j+1/2,j+1/2} \right] = 0. \quad (91)$$

In order to turn these equations into a Robin-type boundary condition, we need to compute the discrete samples $\tilde{\varphi}_{k,m}^{j+1/2,j+1/2}$ by considering the ODEs established for these auxiliary function earlier. Here, we discuss the TR-based discretization of (26) by first employing Fourier expansion: Setting $\rho = 2/\Delta t$ and for $k = 1, 2, \dots, M$, we have

$$\begin{aligned} \frac{\tilde{\varphi}_{k,m}^{j+1,j+1} - \tilde{\varphi}_{k,m}^{j,j+1}}{\Delta t} + \eta_k^2 \frac{\tilde{\varphi}_{k,m}^{j+1,j+1} + \tilde{\varphi}_{k,m}^{j,j+1}}{2} \\ = \frac{\tilde{\varphi}_m^{j+1,j+1} + \tilde{\varphi}_m^{j,j+1}}{2}. \end{aligned} \quad (92)$$

Introduce the scaling $\bar{\eta}_k = \eta_k/\sqrt{\rho}$ so that

$$\begin{aligned} \tilde{\varphi}_{k,m}^{j+1,j+1} &= \frac{(1 - \bar{\eta}_k^2)}{(1 + \bar{\eta}_k^2)} \tilde{\varphi}_{k,m}^{j,j+1} \\ &+ \frac{2/\rho}{(1 + \bar{\eta}_k^2)} \left[\tilde{v}_m^{j+1} + \frac{\tilde{\varphi}_m^{j,j+1} - \tilde{\varphi}_m^{j,j}}{2} \right]. \end{aligned} \quad (93)$$

For the staggered configuration, we have

$$\begin{aligned} \tilde{\varphi}_{k,m}^{j+1/2,j+1/2} &= \frac{1}{2} \left[\left(\frac{1 - \bar{\eta}_k^2}{1 + \bar{\eta}_k^2} \right) \tilde{\varphi}_{k,m}^{j,j+1} + \tilde{\varphi}_{k,m}^{j,j} \right] \\ &+ \frac{1/\rho}{(1 + \bar{\eta}_k^2)} \left[\tilde{v}_m^{j+1} + \frac{\tilde{\varphi}_m^{j,j+1} - \tilde{\varphi}_m^{j,j}}{2} \right]. \end{aligned} \quad (94)$$

The values of $\tilde{\varphi}_{k,m}^{j,j+1}$ and $\tilde{\varphi}_m^{j,j+1}$ can be obtained by propagation along τ_2 using $\tilde{\varphi}_{k,m}^{j,j}$ and $\tilde{\varphi}_m^{j,j}$ as the initial condition:

$$\begin{aligned} \tilde{\varphi}_{k,m}^{j,j+1} &= \frac{(1 - \alpha_2^{-2} m^2)}{(1 + \alpha_2^{-2} m^2)} \tilde{\varphi}_{k,m}^{j,j}, \\ \frac{1}{2} [\tilde{\varphi}_m^{j,j+1} - \tilde{\varphi}_m^{j,j}] &= \frac{-\alpha_2^{-2} m^2}{(1 + \alpha_2^{-2} m^2)} \tilde{\varphi}_m^{j,j}, \quad m \in \mathbb{J}_2. \end{aligned} \quad (95)$$

Next we plug-in the value of $\tilde{\varphi}_{k,m}^{j+1/2,j+1/2}$ in (91) which leads to following compact form of the boundary maps

$$\partial_{y_1} \tilde{v}_m^{j+1} \pm \alpha_1 \varpi \tilde{v}_m^{j+1} = \mp \alpha_1 \tilde{\mathcal{B}}_{m,a_1}^{j+1/2}, \quad (96)$$

where ϖ is same as that in BDF1 and the history functions are given by

$$\begin{aligned} & \tilde{\mathcal{B}}_{m,a_1}^{j+1/2} \\ &= \sum_{k=1}^M \frac{-\bar{b}_k}{2} \left[\left(\frac{1-\bar{\eta}_k^2}{1+\bar{\eta}_k^2} \right) \left(\frac{1-\alpha_2^{-2}m^2}{1+\alpha_2^{-2}m^2} \right) + 1 \right] \tilde{\varphi}_{k,m}^{j,j} \\ &+ \sum_{k=1}^M \frac{\Gamma_k}{\rho} \left(\frac{-\alpha_2^{-2}m^2}{1+\alpha_2^{-2}m^2} \right) \tilde{u}_m^j. \end{aligned} \quad (97)$$

Note that these Robin type maps are written for each component in Fourier series. Also ϖ is independent of m in this case as well which allows us to take inverse Fourier transform of these maps as:

$$\partial_{y_1} v^{j+1} \pm \alpha_1 \varpi v^{j+1} = \mp \alpha_1 \mathcal{B}_{a_1}^{j+1/2}, \quad (98)$$

where

$$\mathcal{B}_{a_1}^{j+1/2}(y_2) = \sum_{J_2} \tilde{\mathcal{B}}_{m,a_1}^{j+1/2} e^{im y_2}, \quad a_1 \in \{r, l\}. \quad (99)$$

5. CP-BDF1

The discrete scheme for the boundary maps is said to be ‘CP–BDF1’ if the temporal derivatives in the realization of the boundary maps, dubbed as ‘CP’, developed in Sec. **II C** are discretized using the one-step method BDF1. To achieve this, we start by writing the time-discrete form of the DtN maps present in (34) in the reference domain as

$$\sqrt{\beta_1} \partial_{y_1} \tilde{u}_m^{j+1} \pm e^{-i\pi/4} \left[b_0 \tilde{u}_m^{j+1} - \sum_{k=1}^M b_k \tilde{\varphi}_{k,m}^{j+1} \right] = 0. \quad (100)$$

In order to turn these equations into a Robin-type boundary condition, we need to compute the discrete samples $\varphi_{k,m}^{j+1}$ by considering the ODEs established for these auxiliary function earlier. Here, we discuss the BDF1-based discretization of (33) by first employing Fourier expansion: Setting $\rho = 1/\Delta t$ and for $k = 1, 2, \dots, M$, we have

$$\begin{aligned} & i \frac{\tilde{\varphi}_{k,m}^{j+1} - \tilde{\varphi}_{k,m}^j}{\Delta t} - (\beta_2 m^2 - i\eta_k^2) \tilde{\varphi}_{k,m}^{j+1} = i \tilde{u}_m^{j+1} \\ & \tilde{\varphi}_{k,m}^{j+1} = \frac{1}{(\rho + i\beta_2 m^2 + \eta_k^2)} \left[\rho \tilde{\varphi}_{k,m}^j + \tilde{u}_m^{j+1} \right]. \end{aligned} \quad (101)$$

Introduce the scaling $\bar{\eta}_k = \eta_k/\sqrt{\rho}$ so that

$$\tilde{\varphi}_{k,m}^{j+1} = \frac{1}{1 + \alpha_2^{-2}m^2 + \bar{\eta}_k^2} \left[\tilde{\varphi}_{k,m}^j + \frac{1}{\rho} \tilde{u}_m^{j+1} \right], \quad (102)$$

where $\tilde{\varphi}_{k,m}^j$ and \tilde{u}_m^j approximate the Fourier coefficients $\mathcal{F}_{y_2}[\varphi_k(y_2, j\Delta t)]$ and $\mathcal{F}_{y_2}[u(y_1, y_2, j\Delta t)]$, respectively. Next we plug-in the value of $\tilde{\varphi}_{k,m}^{j+1}$ in (100) to

obtain the following boundary maps

$$\begin{aligned} & \partial_{y_1} \tilde{u}_m^{j+1} \pm \alpha_1 \varpi_m \tilde{u}_m^{j+1} \\ &= \mp \alpha_1 \sum_{k=1}^M \Gamma_{k,m} \tilde{\varphi}_{k,m}^j = \mp \alpha_1 \tilde{\mathcal{B}}_{m,a_1}^{j+1}, \end{aligned} \quad (103)$$

where we have set $\bar{b}_0 = b_0/\sqrt{\rho}$, $\bar{b}_k = b_k/\sqrt{\rho}$ and

$$\begin{aligned} \varpi_m &= \bar{b}_0 + \frac{1}{\rho} \sum_{k=1}^M \Gamma_{k,m}, \\ \Gamma_{k,m} &= \frac{-\bar{b}_k}{(1 + \alpha_2^{-2}m^2 + \bar{\eta}_k^2)}. \end{aligned} \quad (104)$$

Note that these Robin type maps are written for each component in Fourier series. Also observe that ϖ is m -dependent in this case which poses a difficulty in taking inverse Fourier transform of these maps to express them in physical space.

6. CP-TR

The discrete scheme for the boundary maps is said to be ‘CP–TR’ if the temporal derivatives in the realization of the boundary maps, dubbed as ‘CP’, developed in Sec. **II C** are discretized using the one-step method TR. To achieve this, we start by writing the time-discrete form of the DtN maps present in (34) in the reference domain as

$$\sqrt{\beta_1} \partial_{y_1} \tilde{v}_m^{j+1} \pm e^{-i\pi/4} \left[b_0 \tilde{v}_m^{j+1} - \sum_{k=1}^M b_k \tilde{\varphi}_{k,m}^{j+1/2} \right] = 0. \quad (105)$$

In order to turn these equations into a Robin-type boundary condition, we need to compute the discrete samples $\varphi_{k,m}^{j+1/2}$ by considering the ODEs established for these auxiliary function earlier. Here, we discuss the TR-based discretization of (33) by first employing Fourier expansion: Setting $\rho = 2/\Delta t$ and for $k = 1, 2, \dots, M$, we have

$$\begin{aligned} & i \frac{\tilde{\varphi}_{k,m}^{j+1} - \tilde{\varphi}_{k,m}^j}{\Delta t} - (\beta_2 m^2 - i\eta_k^2) \frac{\tilde{\varphi}_{k,m}^{j+1} + \tilde{\varphi}_{k,m}^j}{2} = i \tilde{v}_m^{j+1} \\ & \tilde{\varphi}_{k,m}^{j+1} = \frac{(\rho - i\beta_2 m^2 - \eta_k^2)}{(\rho + i\beta_2 m^2 + \eta_k^2)} \tilde{\varphi}_{k,m}^j + \frac{2\tilde{v}_m^{j+1}}{(\rho + i\beta_2 m^2 + \eta_k^2)}. \end{aligned}$$

Introduce the scaling $\bar{\eta}_k = \eta_k/\sqrt{\rho}$ so that

$$\tilde{\varphi}_{k,m}^{j+1} = \frac{(1 - \alpha_2^{-2}m^2 - \bar{\eta}_k^2)}{(1 + \alpha_2^{-2}m^2 + \bar{\eta}_k^2)} \tilde{\varphi}_{k,m}^j + \frac{(2/\rho)\tilde{v}_m^{j+1}}{(1 + \alpha_2^{-2}m^2 + \bar{\eta}_k^2)}.$$

For the staggered configuration, we have

$$\tilde{\varphi}_{k,m}^{j+1/2} = \frac{1}{(1 + \alpha_2^{-2}m^2 + \bar{\eta}_k^2)} \left[\tilde{\varphi}_{k,m}^j + (1/\rho)\tilde{v}_m^{j+1} \right].$$

Next we plug-in the value of $\tilde{\varphi}_{k,m}^{j+1/2}$ in (105) to obtain the following boundary maps

$$\partial_{y_1} \tilde{v}_m^{j+1} \pm \alpha_1 \varpi_m \tilde{v}_m^{j+1} = \mp \alpha_1 \tilde{\mathcal{B}}_{m,a_1}^{j+1/2}, \quad (106)$$

where ϖ_m is same as CP-BDF1 and the history function is given by

$$\tilde{\mathcal{B}}_{m,a_1}^{j+1/2} = \left[\sum_{k=1}^M \Gamma_{k,m} \tilde{\varphi}_{k,m}^j \right]_{y_1=y_{a_1}}, \quad a_1 \in \{l, r\}. \quad (107)$$

Also observe that ϖ is m -dependent in this case which poses a difficulty in taking inverse Fourier transform of these maps to express them in physical space.

7. HF-BDF1

The discrete scheme for the boundary maps obtained under high-frequency approximation is said to be ‘HF-CQ-BDF1’ if the underlying one-step method in the CQ scheme is BDF1. Let $\nu \in \{-1/2, +1/2\}$ and $(\omega_k^{(\nu)})_{k \in \mathbb{N}_0}$ denote the corresponding quadrature weights, then the resulting discretization of the DtN maps described in (36) reads as

$$\begin{aligned} \sqrt{\beta_1} \partial_{y_1} u^{j+1} \pm \sqrt{\rho} e^{-i\pi/4} u^{j+1} \mp \frac{e^{i\pi/4}}{2\sqrt{\rho}} \beta_2 \partial_{y_2}^2 u^{j+1} \\ = \mp \sqrt{\rho} e^{-i\pi/4} \mathcal{B}_{a_1,1/2}^{j+1} \pm \frac{e^{i\pi/4}}{2\sqrt{\rho}} \beta_2 \partial_{y_2}^2 \mathcal{B}_{a_1,-1/2}^{j+1}, \end{aligned} \quad (108)$$

where history functions are given by

$$\mathcal{B}_{a_1,\nu}^{j+1} = \sum_{k=1}^{j+1} \omega_k^{(\nu)} u^{j+1-k}, \quad a_1 \in \{l, r\}.$$

Set $\alpha_j = \sqrt{\rho/\beta_j} e^{-i\pi/4}$ for $j = 1, 2$, then the DtN maps can be expressed compactly as

$$\begin{aligned} \partial_{y_1} u^{j+1} \pm \alpha_1 u^{j+1} \mp \frac{1}{2} \alpha_1 \alpha_2^{-2} \partial_{y_2}^2 u^{j+1} \\ = \mp \alpha_1 \mathcal{B}_{a_1,1/2}^{j+1} \pm \frac{1}{2} \alpha_1 \alpha_2^{-2} \partial_{y_2}^2 \mathcal{B}_{a_1,-1/2}^{j+1}. \end{aligned} \quad (109)$$

On account of periodicity along y_2 , we expand the field as a Fourier series and rewrite the DtN maps for each component as

$$\begin{aligned} \partial_{y_1} \tilde{u}_m^{j+1} \pm \alpha_1 \tilde{u}_m^{j+1} \mp \frac{1}{2} \alpha_1 \alpha_2^{-2} m^2 \tilde{u}_m^{j+1} \\ = \mp \alpha_1 \tilde{\mathcal{B}}_{m,a_1,1/2}^{j+1} \pm \frac{1}{2} \alpha_1 \alpha_2^{-2} m^2 \tilde{\mathcal{B}}_{m,a_1,-1/2}^{j+1}. \end{aligned} \quad (110)$$

Under high-frequency approximation, we can express DtN maps as a Robin-type map as

$$\begin{aligned} \partial_{y_1} \tilde{u}_m^{j+1} - \alpha_1 \varpi_m \tilde{u}_m^{j+1} = +\alpha_1 \tilde{\mathcal{B}}_{m,l}^{j+1}, \\ \partial_{y_1} \tilde{u}_m^{j+1} + \alpha_1 \varpi_m \tilde{u}_m^{j+1} = -\alpha_1 \tilde{\mathcal{B}}_{m,r}^{j+1}, \end{aligned} \quad (111)$$

where we introduced $\varpi_m = 1 + \alpha_2^{-2} m^2/2$ and

$$\tilde{\mathcal{B}}_{m,a_1}^{j+1} = \tilde{\mathcal{B}}_{m,a_1,1/2}^{j+1} + \frac{1}{2} \alpha_2^{-2} m^2 \tilde{\mathcal{B}}_{m,a_1,-1/2}^{j+1}. \quad (112)$$

8. HF-TR

The discrete scheme for the boundary maps obtained under high-frequency approximation is said to be ‘HF-CQ-TR’ if the underlying one-step method in the CQ scheme is TR. Let $\nu \in \{-1/2, +1/2\}$ and $(\omega_k^{(\nu)})_{k \in \mathbb{N}_0}$ denote the corresponding quadrature weights, then the resulting discretization of the DtN maps (consistent with staggered samples of the field) described in (36) reads as

$$\begin{aligned} \sqrt{\beta_1} \partial_{y_1} v^{j+1} \pm \sqrt{\rho} e^{-i\pi/4} v^{j+1} \mp \frac{e^{i\pi/4}}{2\sqrt{\rho}} \beta_2 \partial_{y_2}^2 v^{j+1} \\ = \mp \sqrt{\rho} e^{-i\pi/4} \mathcal{B}_{a_1,1/2}^{j+1/2} \pm \frac{e^{i\pi/4}}{2\sqrt{\rho}} \beta_2 \partial_{y_2}^2 \mathcal{B}_{a_1,-1/2}^{j+1/2}, \end{aligned} \quad (113)$$

where the history functions are given by

$$\mathcal{B}_{a_1,\nu}^{j+1/2} = \sum_{k=1}^{j+1} \omega_k^{(\nu)} v^{j+1-k}, \quad a_1 \in \{l, r\}. \quad (114)$$

Following along the similar lines as discussed in BDF1 case, we can obtain a compact Robin-type boundary map as

$$\begin{aligned} \partial_{y_1} \tilde{v}_m^{j+1} - \alpha_1 \varpi_m \tilde{v}_m^{j+1} = +\alpha_1 \tilde{\mathcal{B}}_{m,l}^{j+1/2}, \\ \partial_{y_1} \tilde{v}_m^{j+1} + \alpha_1 \varpi_m \tilde{v}_m^{j+1} = -\alpha_1 \tilde{\mathcal{B}}_{m,r}^{j+1/2}, \end{aligned} \quad (115)$$

where $\varpi_m = 1 + \alpha_2^{-2} m^2/2$ and for $a_1 \in \{r, l\}$

$$\tilde{\mathcal{B}}_{m,a_1}^{j+1/2} = \tilde{\mathcal{B}}_{m,a_1,1/2}^{j+1/2} + \frac{1}{2} \alpha_2^{-2} m^2 \tilde{\mathcal{B}}_{m,a_1,-1/2}^{j+1/2}. \quad (116)$$

Note that ϖ_m is m -dependent which makes it difficult to take inverse Fourier transform of the maps obtained in (115) in order to express them in physical space. This is similar to the case of conventional-Padé approach.

B. Numerical Solution of the IBVP

1. CQ and NP

Having discussed the temporal discretization of the novel boundary maps considered in this work together with that of the interior problem, we would like to address the spatial problem at hand. For spatial discretization, we use a method which is a combination of the Legendre and the Fourier basis within the framework of Galerkin formulation. We construct a boundary-adapted basis in terms of Legendre polynomials which makes it convenient to enforce the boundary conditions and, at the same time, yields a banded linear system. Note that the formulation of the linear system requires a homogeneous form of boundary maps which is achieved by a boundary lifting process. Set $\mathbb{I} = [-1, 1]$ and let $L_n(y)$ denote the Legendre polynomial of degree n . Define the polynomial space

$$P_N = \text{Span} \{L_p(y) \mid p = 0, 1, \dots, N, y \in \mathbb{I}\}. \quad (117)$$

Similarly, using the Fourier basis, we define the linear vector space

$$\mathbb{V}_N = \text{Span} \{ \psi_k = \exp(iky) \mid k \in \mathbb{J}_2, y \in \pi\mathbb{I} \}. \quad (118)$$

where the index set is given by

$$\mathbb{J}_2 = \left\{ -\frac{N}{2}, \dots, \frac{N}{2} - 1 \right\}. \quad (119)$$

For the 2D problem, we consider the tensor product space given by $\mathbb{P}_N \otimes \mathbb{V}_N$. In order to enforce the boundary conditions exactly, we introduce the space of boundary-adapted basis as follows:

$$\mathbb{X}_N = \left\{ u \in \mathbb{P}_N \otimes \mathbb{V}_N \mid \begin{array}{l} (\partial_{y_1} - \kappa)u(y_1, y_2)|_{y_1=-1} = 0, \\ (\partial_{y_1} + \kappa)u(y_1, y_2)|_{y_1=+1} = 0 \end{array} \right\},$$

where κ is determined by the Robin-type formulation of the TBCs specific to the method chosen for the temporal discretization of the boundary maps.

Remark 1. *The form of κ follows from the Robin-type formulation of the discretized version of the DtN-maps as discussed in Sec. IV A. For CQ methods $\kappa = \alpha_1 = \sqrt{\rho/\beta_1} \exp(-i\pi/4)$ while for the NP methods, we have $\kappa = \alpha_1 \varpi$.*

Note that the CQ and NP methods afford the possibility to be casted in this form on account of the fact that ϖ is independent of the m -th Fourier component. But CP and HF methods cannot be casted in this form as they have m -dependent ϖ . The construction of the boundary-adapted basis and boundary lifting process will be discussed for these methods separately. Let the index set $\{0, 1, \dots, N-2\}$ be denoted by \mathbb{J}_1 . For CQ and NP methods, we introduce a function χ to convert the discrete TBCs to a homogeneous form by stating the original field as $w^j = w^j + \chi^j(y_1, y_2)$ where $w^j \in \mathbb{X}_N$ so that

$$\begin{aligned} [-\alpha_1^{-2} \partial_{y_1}^2 - \alpha_2^{-2} \partial_{y_2}^2 + 1](w^{j+1} + \chi^{j+1}) &= w^j, \\ (\partial_{y_1} - \kappa)w^{j+1}|_{y_1=-1} &= 0, \\ (\partial_{y_1} + \kappa)w^{j+1}|_{y_1=+1} &= 0, \end{aligned} \quad (120)$$

and the field $\chi^j(y)$ is forced to satisfy the constraints below

$$\begin{aligned} (\partial_{y_1} - \kappa)\chi^j(y_1, y_2)|_{y_1=-1} &= +\alpha_1 \mathcal{B}_l^j(y_2), \\ (\partial_{y_1} + \kappa)\chi^j(y_1, y_2)|_{y_1=+1} &= -\alpha_1 \mathcal{B}_r^j(y_2). \end{aligned} \quad (121)$$

The form of the equations suggest the use of an ansatz of the form $\chi^j(y_1, y_2) = c_l^j \chi_l^j + c_r^j \chi_r^j$ with $c_l^j = \alpha_1 \mathcal{B}_l^j$ and $c_r^j = -\alpha_1 \mathcal{B}_r^j$ so that the lifting functions satisfy

$$\begin{aligned} (\partial_{y_1} - \kappa) \begin{pmatrix} \chi_l \\ \chi_r \end{pmatrix} \Big|_{y_1=-1} &= \begin{pmatrix} 1 \\ 0 \end{pmatrix}, \\ (\partial_{y_1} + \kappa) \begin{pmatrix} \chi_l \\ \chi_r \end{pmatrix} \Big|_{y_1=+1} &= \begin{pmatrix} 0 \\ 1 \end{pmatrix}. \end{aligned} \quad (122)$$

From here, the degree of the lifting functions $\chi_{l,r}$ can be inferred to be utmost 1. Exploiting the fact that we can expand them in terms of Legendre polynomials, we have

$$\begin{pmatrix} \chi_l(y_1) \\ \chi_r(y_1) \end{pmatrix} = A_0 \begin{pmatrix} L_0(y_1) \\ L_1(y_1) \end{pmatrix}, \quad (123)$$

where A_0 is the unknown transformation matrix. Solving the linear system for A_0 yields

$$\begin{cases} \chi_l(y_1) = -\frac{1}{2\kappa} L_0(y_1) + \frac{1}{2(\kappa+1)} L_1(y_1), \\ \chi_r(y_1) = +\frac{1}{2\kappa} L_0(y_1) + \frac{1}{2(\kappa+1)} L_1(y_1). \end{cases} \quad (124)$$

The lifted field then takes the form

$$w^j = w^j + \alpha_1 \left[\chi_l(y_1) \mathcal{B}_l^j(y_2) - \chi_r(y_1) \mathcal{B}_r^j(y_2) \right], \quad (125)$$

which can be expanded as

$$\begin{aligned} w^j &= w^j - \frac{\alpha_1}{2\kappa} \sum_{q \in \mathbb{J}_2} \left[\tilde{\mathcal{B}}_{q,r}^j + \tilde{\mathcal{B}}_{q,l}^j \right] L_0(y_1) \psi_q(y_2) \\ &\quad - \frac{\alpha_1}{2(1+\kappa)} \sum_{q \in \mathbb{J}_2} \left[\tilde{\mathcal{B}}_{q,r}^j - \tilde{\mathcal{B}}_{q,l}^j \right] L_1(y_1) \psi_q(y_2), \end{aligned} \quad (126)$$

where we have employed the Fourier expansion of the history functions

$$\mathcal{B}_{a_1}^j(y_2) = \sum_{q \in \mathbb{J}_2} \tilde{\mathcal{B}}_{q,a_1}^j \psi_q(y_2), \quad a_1 \in \{l, r\}. \quad (127)$$

Next, we choose the basis $\theta_{p,q} \in \mathbb{X}_N$ defined as

$$\theta_{p,q}(y_1, y_2) = \phi_p(y_1) \psi_q(y_2), \quad p \in \mathbb{J}_1, q \in \mathbb{J}_2, \quad (128)$$

where $\{\phi_p \mid p \in \mathbb{J}_1\}$ can be constructed using the ansatz $\phi_p(y_1) = L_p(y_1) + a_p L_{p+1}(y_1) + b_p L_{p+2}(y_1)$. Imposing the boundary conditions in the definition of \mathbb{X}_N , the sequences $(a_p)_{p \in \mathbb{J}_1}$ and $(b_p)_{p \in \mathbb{J}_1}$ work out to be

$$a_p = 0, \quad b_p = -\frac{\kappa + \frac{1}{2}p(p+1)}{\kappa + \frac{1}{2}(p+2)(p+3)}, \quad p \in \mathbb{J}_1. \quad (129)$$

The testing functions for the variational formulation in context of a Galerkin method can now be stated as

$$\tilde{\theta}_{p,q}(y_1, y_2) = \phi_p(y_1) \psi_q^*(y_2) = \phi_p(y_1) \psi_{-q}(y_2). \quad (130)$$

The mass matrix and the stiffness matrix for the boundary-adapted Legendre basis are denoted by $M_1 = (\mathbf{m}_{k,j}^{(1)})_{k,j \in \mathbb{J}_1}$ and $S_1 = (\mathbf{s}_{k,j}^{(1)})_{k,j \in \mathbb{J}_1}$, respectively, where

$$\begin{aligned} \mathbf{s}_{j,k}^{(1)} &= -(\phi_j, \phi_k)_{\mathbb{I}} = \begin{cases} -2(2k+3)b_k, & j = k, \\ 0, & \text{otherwise,} \end{cases} \\ \mathbf{m}_{j,k}^{(1)} &= (\phi_j, \phi_k)_{\mathbb{I}} = \begin{cases} \frac{2b_{k-2}}{2k+1}, & j = k-2, \\ \frac{2}{2k+1} + \frac{2b_k^2}{2k+5}, & j = k, \\ \frac{2b_k}{2k+5}, & j = k+2, \\ 0 & \text{otherwise.} \end{cases} \end{aligned} \quad (131)$$

The mass matrix and the stiffness matrix for the Fourier basis are denoted by $M_2 = (\mathbf{m}_{k,j}^{(2)})_{k,j \in \mathbb{J}_2}$ and $S_2 = (\mathbf{s}_{k,j}^{(2)})_{k,j \in \mathbb{J}_2}$, respectively, where

$$\begin{aligned} \mathbf{s}_{j,k}^{(2)} &= -(\psi_j'', \psi_k^*)_{\pi\mathbb{I}} = \begin{cases} 2\pi k^2 & , k = j \\ 0 & , \text{otherwise,} \end{cases} \\ \mathbf{m}_{j,k}^{(2)} &= (\psi_j, \psi_k^*)_{\pi\mathbb{I}} = \begin{cases} 2\pi, & k = j, \\ 0, & \text{otherwise.} \end{cases} \end{aligned} \quad (132)$$

Within the variational formulation, our goal is to find the approximate solution $u_N \in \mathbf{X}_N$ to (65) such that

$$\begin{aligned} -\alpha_1^{-2} \left(\partial_{y_1}^2 u_N^{j+1}, \tilde{\theta}_{p,q} \right)_{\Omega_i^{\text{ref}}} - \alpha_2^{-2} \left(\partial_{y_2}^2 u_N^{j+1}, \tilde{\theta}_{p,q} \right)_{\Omega_i^{\text{ref}}} \\ + \left(u_N^{j+1}, \tilde{\theta}_{p,q} \right)_{\Omega_i^{\text{ref}}} = \left(u_N^j, \tilde{\theta}_{p,q} \right)_{\Omega_i^{\text{ref}}}, \end{aligned} \quad (133)$$

for every $\tilde{\theta}_{p,q} \in \mathbf{X}_N$ where $(u, \tilde{\theta})_{\Omega_i^{\text{ref}}} = \int_{\Omega_i^{\text{ref}}} u \tilde{\theta} d^2 \mathbf{y}$ is the scalar product in $L^2(\Omega_i^{\text{ref}})$. We approximate u by polynomial interpolation over the Legendre-Gauss-Lobatto (LGL) nodes in the context of discrete Legendre transforms. The variational formulation (133) in terms of the unknown field w^{j+1} (dropping the subscript 'N' for the sake of brevity) can now be stated as

$$\begin{aligned} - \left[\alpha_1^{-2} \left(\partial_{y_1}^2 w^{j+1}, \tilde{\theta}_{p,q} \right) + \alpha_2^{-2} \left(\partial_{y_2}^2 w^{j+1}, \tilde{\theta}_{p,q} \right) \right] \\ + \left(w^{j+1}, \tilde{\theta}_{p,q} \right) = \left(w^j, \tilde{\theta}_{p,q} \right) + \mathcal{I}, \end{aligned} \quad (134)$$

where

$$\begin{aligned} \mathcal{I} &= - \left(\chi^{j+1}, \tilde{\theta}_{p,q} \right) + \underbrace{\alpha_1^{-2} \left(\partial_{y_1}^2 \chi^{j+1}, \tilde{\theta}_{p,q} \right)}_{=0} \\ &\quad + \alpha_2^{-2} \left(\partial_{y_2}^2 \chi^{j+1}, \tilde{\theta}_{p,q} \right). \end{aligned} \quad (135)$$

The non-zero term above works out to be

$$\begin{aligned} \partial_{y_2}^2 \chi^{j+1} &= -\alpha_1 \chi_r(y_1) \partial_{y_2}^2 \mathcal{B}_r^{j+1}(y_2) \\ &\quad + \alpha_1 \chi_l(y_1) \partial_{y_2}^2 \mathcal{B}_l^{j+1}(y_2). \end{aligned} \quad (136)$$

Integration by parts for $a_1 \in \{l, r\}$ yields

$$\left(\chi_{a_1} \partial_{y_2}^2 \mathcal{B}_{a_1}^{j+1}, \tilde{\theta}_{p,q} \right) = -q^2 \left(\chi_{a_1} \mathcal{B}_{a_1}^{j+1}, \tilde{\theta}_{p,q} \right), \quad (137)$$

so that

$$\mathcal{I} = \alpha_1 (1 + \alpha_2^{-2} q^2) \left[(\mathcal{B}_r^{j+1} \chi_r, \tilde{\theta}_{p,q}) - (\mathcal{B}_l^{j+1} \chi_l, \tilde{\theta}_{p,q}) \right]. \quad (138)$$

Let $\tilde{u}_{p,q}$ denote the expansion coefficients of the field in Legendre-Fourier basis and $\hat{w}_{p,q}$ denote the expansion co-

efficients in the boundary-adapted basis as

$$\begin{aligned} w^j(\mathbf{y}) &= \sum_{p \in \mathbb{J}_1, q \in \mathbb{J}_2} \hat{w}_{p,q}^j \theta_{p,q}(\mathbf{y}), \\ &= \sum_{p=0}^N \sum_{q \in \mathbb{J}_2} \tilde{w}_{p,q}^j L_p(y_1) \psi_q(y_2), \\ u^j(\mathbf{y}) &= \sum_{p=0}^N \sum_{q \in \mathbb{J}_2} \tilde{u}_{p,q}^j L_p(y_1) \psi_q(y_2). \end{aligned} \quad (139)$$

Let us introduce the matrices $\widehat{W} = (\hat{w}_{p,q})$ and $\tilde{U} = (\tilde{u}_{p,q})$ for convenience. In matrix form, the expansion coefficients for the fields in the Legendre basis assume the form

$$\begin{aligned} \tilde{U}^j &= \tilde{W}^j - \frac{\alpha_1}{2\kappa} \mathbf{e}_0 \otimes \left[\tilde{\mathcal{B}}_r^j + \tilde{\mathcal{B}}_l^j \right]^\top \\ &\quad - \frac{\alpha_1}{2(1+\kappa)} \mathbf{e}_1 \otimes \left[\tilde{\mathcal{B}}_r^j - \tilde{\mathcal{B}}_l^j \right]^\top, \end{aligned} \quad (140)$$

where $\tilde{\mathcal{B}}_{a_1}^j$, $a_1 \in \{l, r\}$, are the corresponding Fourier coefficients. The inner-products in the variational form involving the stiffness-matrix follows from

$$\begin{aligned} - \left[\alpha_1^{-2} \left(\partial_{y_1}^2 w^{j+1}, \tilde{\theta}_{p,q} \right) + \alpha_2^{-2} \left(\partial_{y_2}^2 w^{j+1}, \tilde{\theta}_{p,q} \right) \right] \\ = \sum_{p',q'} \left[\alpha_1^{-2} \mathbf{s}_{p,p'}^{(1)} \hat{w}_{p',q'}^{j+1} \mathbf{m}_{q',q}^{(2)} + \alpha_2^{-2} \mathbf{m}_{p,p'}^{(1)} \hat{w}_{p',q'}^{j+1} \mathbf{s}_{q',q}^{(2)} \right] \\ = \left(\alpha_1^{-2} S_1 \widehat{W}^{j+1} M_2 + \alpha_2^{-2} M_1 \widehat{W}^{j+1} S_2 \right)_{p,q}, \end{aligned} \quad (141)$$

and that involving only the mass-matrices follow from

$$\begin{aligned} (w^{j+1}, \tilde{\theta}_{p,q}) &= \sum_{p',q'} \mathbf{m}_{p,p'}^{(1)} \hat{w}_{p',q'}^{j+1} \mathbf{m}_{q',q}^{(2)} \\ &= \left(M_1 \widehat{W}^{j+1} M_2 \right)_{p,q}. \end{aligned} \quad (142)$$

We can further simplify the expression for the linear system by collecting the right hand side of (134) into one term. To this end, let $f^j(y_1, y_2)$ be such that $(w^j, \tilde{\theta}_{p,q}) + \mathcal{I} = (f^j, \tilde{\theta}_{p,q})$, then it follows that

$$\begin{aligned} \frac{\alpha_1}{4\pi} \sum_{q \in \mathbb{J}_2} (1 + \alpha_2^{-2} q^2) \left(\frac{g_{q,+}^j}{\kappa} + \frac{g_{q,-}^j}{1+\kappa} \right) L_0(y_1) \psi_q(y_2) \\ + u^j = f^j, \end{aligned} \quad (143)$$

where $g_{q,\pm}^j = (\mathcal{B}_r^{j+1} \pm \mathcal{B}_l^{j+1}, \psi_q^*)_{\pi\mathbb{I}}$. Introducing the diagonal matrix $\mathcal{D}_2 = \text{diag} \left(\{1 + \alpha_2^{-2} q^2\}_{q \in \mathbb{J}_2} \right)$, the discrete representation of f^j in the matrix form works out to be

$$\begin{aligned} \tilde{F}^j &= \tilde{U}^j + \frac{\alpha_1}{2\kappa} \mathbf{e}_0 \otimes \left[\tilde{\mathcal{B}}_r^{j+1} + \tilde{\mathcal{B}}_l^{j+1} \right]^\top \mathcal{D}_2 \\ &\quad + \frac{\alpha_1}{2(1+\kappa)} \mathbf{e}_1 \otimes \left[\tilde{\mathcal{B}}_r^{j+1} - \tilde{\mathcal{B}}_l^{j+1} \right]^\top \mathcal{D}_2. \end{aligned} \quad (144)$$

The inner product $(f^j, \tilde{\theta}_{p,q})$ can be computed from the knowledge of the Legendre coefficients of the field \tilde{F}^j using the specific form of the boundary-adapted basis. This can be achieved via *quadrature matrix* given in A. The linear system for (134) thus becomes

$$\alpha_1^{-2} S_1 \widehat{W}^{j+1} M_2 + \alpha_2^{-2} M_1 \widehat{W}^{j+1} S_2 + M_1 \widehat{W}^{j+1} M_2 = Q_1 \Gamma \tilde{F}^j M_2, \quad (145)$$

which is recasted as follows

$$(\alpha_1^{-2} M_2 \otimes S_1 + \alpha_2^{-2} S_2 \otimes M_1 + M_2 \otimes M_1) \widehat{\mathbf{w}}^{j+1} = \widehat{\mathbf{f}}^j,$$

where \otimes denotes the tensor product and $\widehat{\mathbf{w}}$, $\widehat{\mathbf{f}}$ denote the column vectors obtained by stacking columns of matrices \widehat{W} , \widehat{F} , respectively, below one another. The mass and stiffness matrices are defined in (131) and the linear system is then solved using LU-decomposition method.

2. CP and HF

For CP and HF methods, we have the following form of the TBCs casted as Robin-type boundary maps:

$$\partial_{y_1} \tilde{u}_m^{j+1} \pm \alpha_1 \varpi_m \tilde{u}_m^{j+1} = \mp \alpha_1 \tilde{\mathcal{B}}_{m,a_1}^{j+1}, \quad a_1 \in \{r, l\}. \quad (146)$$

Note that these maps have m -dependent ϖ which makes it difficult to take the inverse Fourier transform in order to express them in physical space. On account of this fact, we will have to discuss the boundary lifting and basis construction for each Fourier component separately. In order to enforce these m -dependent boundary maps exactly, we define the space of boundary-adapted basis as

$$\mathbb{W}_N = \left\{ \tilde{u}_m \in \mathbb{P}_N \mid \begin{array}{l} (\partial_{y_1} - \kappa_m) \tilde{u}_m(y_1)|_{y_1=-1} = 0, \\ (\partial_{y_1} + \kappa_m) \tilde{u}_m(y_1)|_{y_1=+1} = 0 \end{array} \right\},$$

where κ_m will be determined by the Robin-type formulation of TBCs specific to CP and HF methods. We introduce a function χ_m to convert the discrete BCs to a homogeneous form by stating the original field as $\tilde{u}_m^j = \tilde{w}_m^j + \chi_m^j(y_1)$ where $\tilde{w}_m^j \in \mathbb{W}_N$ so that

$$\begin{aligned} [-\alpha_1^{-2} \partial_{y_1}^2 + \alpha_2^{-2} m^2 + 1] (\tilde{w}_m^{j+1} + \chi_m^{j+1}) &= \tilde{u}_m^j, \\ (\partial_{y_1} - \kappa_m) \tilde{w}_m^{j+1}|_{y_1=-1} &= 0, \\ (\partial_{y_1} + \kappa_m) \tilde{w}_m^{j+1}|_{y_1=+1} &= 0, \end{aligned} \quad (147)$$

and the field $\chi_m^j(y_1)$ is forced to satisfy the constraints:

$$\begin{aligned} (\partial_{y_1} - \kappa_m) \chi_m^j(y_1)|_{y_1=-1} &= +\alpha_1 \tilde{\mathcal{B}}_{m,l}^j, \\ (\partial_{y_1} + \kappa_m) \chi_m^j(y_1)|_{y_1=+1} &= -\alpha_1 \tilde{\mathcal{B}}_{m,r}^j, \end{aligned} \quad (148)$$

Following in the similar manner as in CQ and NP case, the lifting functions for this case works out to be

$$\begin{cases} \chi_{m,l}(y_1) = -\frac{1}{2\kappa_m} L_0(y_1) + \frac{1}{2(\kappa_m + 1)} L_1(y_1), \\ \chi_{m,r}(y_1) = +\frac{1}{2\kappa_m} L_0(y_1) + \frac{1}{2(\kappa_m + 1)} L_1(y_1). \end{cases} \quad (149)$$

The lifted field becomes

$$\tilde{u}_m^j(y_1) = \tilde{w}_m^j(y_1) + \alpha_1 \chi_{m,l} \tilde{\mathcal{B}}_{m,l}^j - \alpha_1 \chi_{m,r} \tilde{\mathcal{B}}_{m,r}^j, \quad (150)$$

which can be expanded as

$$\begin{aligned} \tilde{u}_m^j(y_1) &= \tilde{w}_m^j(y_1) - \frac{\alpha_1}{2\kappa_m} \left[\tilde{\mathcal{B}}_{q,r}^j + \tilde{\mathcal{B}}_{q,l}^j \right] L_0(y_1) \\ &\quad - \frac{\alpha_1}{2(1 + \kappa_m)} \left[\tilde{\mathcal{B}}_{q,r}^j - \tilde{\mathcal{B}}_{q,l}^j \right] L_1(y_1). \end{aligned} \quad (151)$$

Next we address the construction of the basis $\theta_{p,m} \in \mathbb{W}_N$ for the boundary-adapted space \mathbb{W}_N as

$$\theta_{p,m}(y_1) = \phi_{p,m}(y_1), \quad p \in \mathbb{J}_1, \quad m \in \mathbb{J}_2, \quad (152)$$

where $\phi_{p,m}$ can be computed using the ansatz $\phi_{p,m}(y_1) = L_p(y_1) + a_{p,m} L_{p+1}(y_1) + b_{p,m} L_{p+2}(y_1)$. Imposing the boundary conditions in the definition, the sequences $\{a_{p,m}\}$ and $\{b_{p,m}\}$ work out to be

$$a_{p,m} = 0, \quad b_{p,m} = -\frac{\alpha_1 \varpi_m + \frac{1}{2} p(p+1)}{\alpha_1 \varpi_m + \frac{1}{2} (p+2)(p+3)}. \quad (153)$$

The testing functions for the variational formulation in context of a Galerkin method can now be stated as

$$\tilde{\theta}_{p,m}(y_1) = \phi_{p,-m}(y_1) = \phi_{p,m}(y_1), \quad (154)$$

where we used $\varpi_{-m} = \varpi_m$ and $p \in \mathbb{J}_1$, $m \in \mathbb{J}_2$. The mass matrix and the stiffness matrix for the boundary adapted Legendre basis (specific to each m -th Fourier component) are denoted by $\tilde{\mathbf{M}}_{m,1} = (\mathbf{m}_{p,p',m}^{(1)})_{p,p' \in \mathbb{J}_1}$ and $\tilde{\mathbf{S}}_{m,1} = (\mathbf{s}_{p,p',m}^{(1)})_{p,p' \in \mathbb{J}_1}$, respectively, where

$$\begin{aligned} \mathbf{s}_{p,p',m}^{(1)} &= -(\phi_{p',m}, \phi_{p,m}'')_{\mathbb{I}} \\ &= \begin{cases} -2(2p+3)b_{p,m}, & p' = p, \\ 0, & \text{otherwise} \end{cases}, \\ \mathbf{m}_{p,p',m}^{(1)} &= (\phi_{p',m}, \phi_{p,m})_{\mathbb{I}} \\ &= \begin{cases} \frac{2b_{p-2,m}}{2p+1}, & p' = p-2, \\ \frac{2}{2p+1} + \frac{2b_{p,m}^2}{2p+5}, & p' = p, \\ \frac{2b_{p,m}}{2p+5}, & p' = p+2, \\ 0 & \text{otherwise,} \end{cases} \end{aligned} \quad (155)$$

Following along the similar lines as discussed in CQ and NP methods, the variational formulation works out to be

$$\begin{aligned} -\alpha_1^{-2} \left(\partial_{y_1}^2 \tilde{w}_m^{j+1}, \tilde{\theta}_{pm} \right) + (1 + \alpha_2^{-2} m^2) \left(\tilde{w}_m^{j+1}, \tilde{\theta}_{pm} \right) \\ = (\tilde{u}_m^j, \tilde{\theta}_{pm}) + \mathcal{I} \end{aligned} \quad (156)$$

where

$$\mathcal{I} = \alpha_1 (1 + \alpha_2^{-2} m^2) \left[(\tilde{\mathcal{B}}_{m,r}^{j+1} \chi_{m,r}, \tilde{\theta}_{pm}) - (\tilde{\mathcal{B}}_{m,l}^{j+1} \chi_{m,l}, \tilde{\theta}_{pm}) \right].$$

To further simplify the terms on right hand side, let \tilde{f}_m^j be such that

$$(1 + \alpha_2^{-2} m^2) [\alpha_1 \tilde{\mathcal{B}}_{m,r}^{j+1} \tilde{\chi}_{m,r}(y_1) - \alpha_1 \tilde{\mathcal{B}}_{m,l}^{j+1} \tilde{\chi}_{m,l}(y_1)] + \tilde{u}_m^j = \tilde{f}_m^j, \quad (157)$$

then it follows that

$$\tilde{f}_m^j = \tilde{u}_m^j + \frac{\alpha_1 \mathcal{D}_m}{2\kappa_m} \left[\tilde{\mathcal{B}}_{m,r}^{j+1} + \tilde{\mathcal{B}}_{m,l}^{j+1} \right] L_0(y_1) + \frac{\alpha_1 \mathcal{D}_m}{2(1 + \kappa_m)} \left[\tilde{\mathcal{B}}_{m,r}^{j+1} - \tilde{\mathcal{B}}_{m,l}^{j+1} \right] L_1(y_1), \quad (158)$$

where $\mathcal{D}_m = (1 + \alpha_2^{-2} m^2)$. Let $\tilde{u}_{p,m}$ denote the expansion coefficients of the field \tilde{u}_m in Legendre basis for each m -th Fourier component and $\tilde{w}_{p,m}$ denote the expansion coefficients in the boundary-adapted basis as

$$\begin{aligned} \tilde{w}_m^{j+1} &= \sum_{p \in \mathbb{J}_1} \hat{w}_{p,m}^{j+1} \theta_{p,m}(y_1) = \sum_{p' \in \mathbb{J}_1} \hat{w}_{p',m}^{j+1} \phi_{p',m}(y_1), \\ \tilde{u}_m^j &= \sum_{p=0}^N \tilde{u}_{p,m}^{j+1} L_p(y_1). \end{aligned} \quad (159)$$

The inner product $(\tilde{f}_m^j, \tilde{\theta}_{p,m})$ can be computed from the knowledge of the Legendre coefficients of the field \tilde{f}_m^j using the specific form of the boundary-adapted basis. This can be achieved via *quadrature matrix* given in A. The linear system thus becomes

$$\left[\alpha_1^{-2} \tilde{\mathcal{S}}_{m,1} + (1 + \alpha_2^{-2} m^2) \tilde{\mathcal{M}}_{m,1} \right] \hat{\tilde{w}}_m^{j+1} = \tilde{\mathcal{Q}}_{m,1} \Gamma \tilde{\mathcal{f}}_m^j.$$

Introducing the matrices

$$\begin{cases} S_1 = \text{diag} \left(\left\{ \tilde{\mathcal{S}}_{m,1} \right\}_{m \in \mathbb{J}_2} \right), \\ M_1 = \text{diag} \left(\left\{ (1 + \alpha_2^{-2} m^2) \tilde{\mathcal{M}}_{m,1} \right\}_{m \in \mathbb{J}_2} \right), \\ Q_1 = \text{diag} \left(\left\{ \tilde{\mathcal{Q}}_{m,1} \Gamma \right\}_{m \in \mathbb{J}_2} \right), \end{cases} \quad (160)$$

we can rewrite the linear system as

$$[\alpha_1^{-2} S_1 + M_1] \hat{\tilde{w}}^{j+1} = Q_1 \tilde{\mathcal{f}}^j, \quad (161)$$

where $\hat{\tilde{w}}$ and $\tilde{\mathcal{f}}$ denote the block column vectors obtained by stacking the column vectors $\hat{\tilde{w}}_m$ and $\tilde{\mathcal{f}}_m$, respectively, below one another for each m -th Fourier component. The linear system is then solved using LU-decomposition method.

V. NUMERICAL EXPERIMENTS-2D

In this section, we will carry out the extensive numerical tests to showcase the accuracy of the numerical

schemes developed in this work to solve the IBVP (14), focusing on the case $\beta = +1$. We start by analyzing the behaviour of the exact solutions for the IBVP under consideration followed by studying the error evolution behaviour and convergence analysis of the numerical schemes.

A. Exact solutions

The exact solutions admissible for our numerical experiments are such that the initial profile must be effectively supported within the computational domain. We primarily consider the wavepackets which are a modulation of a Gaussian envelop so that the requirement of effective initial support can be easily met. In this class of solutions, we consider the Fourier-Chirped-Gaussian and the Fourier-Hermite-Gaussian profiles.

1. Fourier-Chirped-Gaussian profile

Introduce the parameters $a \in \mathbb{R}_+$ and $b \in \mathbb{R}$ to define the function $\mathcal{G} = \mathcal{G}(x, t; a, b)$ by

$$\mathcal{G} = \frac{1}{\sqrt{1 + 4i(a + ib)t}} \exp \left[\frac{-(a + ib)}{1 + 4i(a + ib)t} x^2 \right]. \quad (162)$$

The family of solutions referred to as Fourier-chirped-Gaussian profile is then given by

$$\begin{aligned} G(\mathbf{x}, t; a, b, c, \zeta) &= \mathcal{G}(x_1 - c_1 t, t; a, b) \\ &\exp \left(+i \frac{1}{2} c x_1 - i \frac{1}{4} c^2 t \right) \exp(i \zeta x_2 - i \zeta^2 t), \end{aligned} \quad (163)$$

where $a \in \mathbb{R}_+$ determines the effective support of the profile at $t = 0$, $b \in \mathbb{R}$ is the *chirp* parameter, $\zeta \in \mathbb{R}$ is the *Fourier spectral* parameter and $c \in \mathbb{R}$ is the *speed* of the profile. Using linear combination, one can further define a more general family of solutions with parameters $A_0, c_0 \in \mathbb{R}$, $(a_j \in \mathbb{R}_+)_{j=1}^n$, $(b_j \in \mathbb{R})_{j=1}^n$ and $(\zeta_j \in \mathbb{R})_{j=1}^n$ given by

$$\begin{aligned} G(\mathbf{x}, t; c_0, A_0; (a_j)_{j=1}^n, (b_j)_{j=1}^n, (\zeta_j)_{j=1}^n) \\ = A_0 \sum_{j=1}^n G(\mathbf{x}, t; a_j, b_j, c_j, \zeta_j), \end{aligned} \quad (164)$$

The specific values of the parameters of the solutions used in the numerical experiments can be summarized as in Table I. The energy content of the profile within the computational domain Ω_i over time is

$$E_{\Omega_i}(t) = \int_{\Omega_i} |G(\mathbf{x}, t)|^2 d^2 \mathbf{x} / \int_{\Omega_i} |G(\mathbf{x}, 0)|^2 d^2 \mathbf{x}. \quad (165)$$

The profiles are chosen with non-zero speed c_0 so that the field hits the boundary of Ω_i .

TABLE I. Fourier-Chirped-Gaussian profile with $A_0 = 2$ and $c_0 \in \{4, 8, 12, 16\}$.

$G(\mathbf{x}, t) = A_0 \sum_{j=1}^n G(x_j, t; a_j, b_j, c_j, \zeta_j), \quad c_j = \text{sgn}(c_j)c_0 \quad \zeta_j = (\pi/d)K_j$					
Type	n	$(a_j \in \mathbb{R})_{j=1}^n$	$(b_j \in \mathbb{R})_{j=1}^n$	$(s_j = \text{sgn}(c_j))_{j=1}^n$	$(K_j \in \mathbb{Z})_{j=1}^n$
I	2	$a_1 = 1/2.5,$	1/2	$s_1 = +1,$	$K_1 = +2,$
		$a_2 = 1/2.3$		$s_2 = -1$	$K_2 = -2$
II	4	$a_1 = 1/2.5,$	1/2	$s_1 = +1,$	$K_1 = +2,$
		$a_2 = 1/2.3,$		$s_2 = -1,$	$K_2 = -2,$
		$a_3 = 1/2.2,$		$s_3 = +1,$	$K_3 = +4,$
		$a_4 = 1/2.4$		$s_4 = -1$	$K_4 = -4$

2. Fourier-Hermite-Gaussian profile

Consider the class of normalized Hermite-Gaussian functions defined by

$$\mathcal{G}_m(x, t; a) = \gamma_m^{-1} H_m \left(\frac{\sqrt{2a}x}{w(t)} \right) \sqrt{\frac{\mu(t)}{a}} \exp[-\mu(t)x^2 - im\theta(t)],$$

where $a > 0$, $m \in \mathbb{N}_0$, $w(t) = \sqrt{1 + (4at)^2}$ and

$$\frac{1}{\mu(t)} = \frac{1}{a} + i4t = \frac{1}{a} w(t) \exp[i\theta(t)],$$

with the normalization factor: $\gamma_m^2 = 2^m (m!) \sqrt{\pi} (2a)^{-1/2}$.

The Hermite polynomials are evaluated using the following relations

$$\begin{aligned} H_{n+1}(x) &= 2xH_n(x) - 2nH_{n-1}(x), \\ H'_{n+1}(x) &= 2(n+1)H_n(x), \end{aligned} \quad (166)$$

with $H_0(x) = 1$ and $H_1(x) = 2x$. Using these functions, we can define a family of solutions referred to as Fourier-Hermite-Gaussian profile by

$$\begin{aligned} G(\mathbf{x}, t; m, a, c) &= \mathcal{G}_{m_1}(x_1 - c_1 t, t; a_1) \\ &\exp\left(+i\frac{1}{2}cx - i\frac{1}{4}c^2 t\right) \exp(i\zeta x_2 - i\zeta^2 t), \end{aligned} \quad (167)$$

where $m \in \mathbb{N}_0$ is the order parameter, $a \in \mathbb{R}_+$ determines the effective support of the profile at $t = 0$, $\zeta \in \mathbb{C}$ is the *spectral* parameter and $c \in \mathbb{R}$ is the velocity of the profile. Once again, using linear combination, one can further define a more general family of solutions with parameters $A_0, c_0 \in \mathbb{R}$, $(m_j \in \mathbb{N}_0)_{j=1}^n$, $(\zeta_j \in \mathbb{C})_{j=1}^n$, and $(a_j \in \mathbb{R}_+)_{j=1}^n$ given by

$$\begin{aligned} G(\mathbf{x}, t; c_0, A_0; (m_j)_{j=1}^n, (a_j)_{j=1}^n, (\zeta_j)_{j=1}^n) \\ = A_0 \sum_{j=1}^n G(\mathbf{x}, t; m_j, a_j, c_j, \zeta_j). \end{aligned} \quad (168)$$

The specific values of the parameters of the solutions used in the numerical experiments can be summarized as in Table II. The profiles are chosen with non-zero speed c_0 so that the field hits the boundary of Ω_i .

B. Tests for evolution error

In this section, we consider the IBVP in (14) where the initial condition corresponds to the exact solutions described in Sec. VA. The error in the evolution of the profile computed numerically is quantified by the relative $L^2(\Omega_i)$ -norm:

$$e(t_j) = \frac{\left(\int_{\Omega_i} |u(\mathbf{x}, t_j) - [u(\mathbf{x}, t_j)]_{\text{num.}}|^2 d^2\mathbf{x} \right)^{1/2}}{\left(\int_{\Omega_i} |u_0(\mathbf{x})|^2 d^2\mathbf{x} \right)^{1/2}}, \quad (169)$$

for $t_j \in [0, T_{max}]$. The integral above will be approximated by Gauss quadrature over LGL-points.

In this work, we have developed four discrete versions of the DtN maps, namely, CQ, NP, CP and HF. Each of these methods have a variant determined by the choice of one-step method used in the temporal discretization so that the complete list of methods to be tested can be labelled as CQ-BDF1, NP-BDF1, CP-BDF1, HF-BDF1 (corresponding to the one-step method BDF1), and, CQ-TR, NP-TR, CP-TR, HF-TR (corresponding to the one-step method TR). For the Padé approximant based methods ‘NP’ and ‘CP’, we distinguish the diagonal approximant of order 20 from that of 50 via the labels ‘NP20’, ‘CP20’ and ‘NP50’, ‘CP50’. The numerical parameters used in this section are summarized in Table III. The exact solutions used are described in Sec. VA.

The numerical results for the evolution error on Ω_i corresponding to the Fourier-chirped-Gaussian and the Fourier-Hermite-Gaussian profiles are shown in Fig. 7. It can be seen that the diagonal Padé approximants based method, namely, NP and CP, perform equally well as compared to that of the convolution quadrature based method. Observe that the TR methods perform better than the BDF1 methods which is clear from the error peaks in Fig. 7. Further, note that the error curves for HF-TR starts separating from the rest just after certain initial time-steps. Also, the performance of HF methods seems to improve for the case of faster moving profiles. For rest of the methods, the accuracy deteriorates with increase in the value of c which can be seen from the error peaks in the Fig. 7. For faster moving profiles,

TABLE II. Fourier-Hermite-Gaussian profile with $A_0 = 2$ and $c_0 \in \{4, 8, 12, 16\}$.
$$G(\mathbf{x}, t) = A_0 \sum_{j=1}^n G(x_1, t; a_j, m_j, c_j, \zeta_j), \quad c_j = \text{sgn}(c_j)c_0 \quad \zeta_j = (\pi/d)K_j$$

Type	n	$(a_j \in \mathbb{R})_{j=1}^n$	$(m_j \in \mathbb{N}_0)_{j=1}^n$	$(s_j = \text{sgn}(c_j))_{j=1}^n$	$(K_j \in \mathbb{Z})_{j=1}^n$
I	2	$a_1 = 1/2.5,$	$m_1 = 1,$	$s_1 = +1,$	$K_1 = +2,$
		$a_2 = 1/2.3$	$m_2 = 2$	$s_2 = -1$	$K_2 = -2$
II	4	$a_1 = 1/2.5,$	$m_1 = 1,$	$s_1 = +1,$	$K_1 = +2,$
		$a_2 = 1/2.3,$	$m_2 = 2,$	$s_2 = -1,$	$K_2 = -2,$
		$a_3 = 1/2.2,$	$m_3 = 1,$	$s_3 = +1,$	$K_3 = +4,$
		$a_4 = 1/2.4$	$m_4 = 2$	$s_4 = -1$	$K_4 = -4$

TABLE III. Numerical parameters for studying the evolution error

Computational domain (Ω_i)	$(-10, 10) \times [-\pi, \pi]$
Maximum time (T_{max})	5
No. of time-steps (N_t)	5000 + 1
Time-step (Δt)	$10^{-3} = T_{max}/(N_t - 1)$
Number of LGL-points ($(N + 1) \times (N + 1)$)	200 × 200

the performance of CP50–TR turns out to be superior than the NP50–TR and CQ–TR. Also, NP20–TR and CP20–TR seems to be least accurate among TR methods which can be attributed to lower order of the Padé approximant chosen. There is no significant difference in the results for evolution error on Ω_i corresponding to the Fourier-chirped-Gaussian profile and the Fourier-Hermite-Gaussian profile.

C. Tests for convergence

In this section, we analyze the convergence behaviour of the numerical schemes for the IBVP in (14) where the initial condition corresponds to the exact solutions described in Sec. V A. The error used to study the convergence behaviour is quantified by the maximum relative $L^2(\Omega_i)$ -norm:

$$e = \max \{e(t_j) | j = 0, 1, \dots, N_t - 1\}, \quad (170)$$

for $t_j \in [0, T_{max}]$. The Table IV lists the numerical parameters for studying the convergence behaviour of CQ, NP, CP and HF methods. The numerical solution is labelled as described in Sec. V B.

The numerical results for the convergence behaviour on Ω_i corresponding to the Fourier-chirped-Gaussian and the Fourier-Hermite-Gaussian profiles are shown in Fig. 8. It can be seen that all the methods under consideration for the convergence tests show stable behaviour for the parameters specified in Table IV. In the log-log scale, we can clearly identify the error curve to be a

straight line before it plateaus. The empirical orders can be recovered from the slope which we found consistent with the order of the underlying one-step method. The TR methods perform better than the BDF1 methods which is obvious from the slope of the error curves in Fig. 8. Particularly for the HF methods, we note that the error background decreases with increase in the value of c as one would expect with the case of high-frequency approximation of the TBCs. Also observe that CP20 methods starts plateauing after a certain number of time-steps unlike CP50. This can be attributed to the approximate nature of the TBCs with a lower order of diagonal approximants chosen. Finally, let us observe that there is no significant difference in the results for convergence on Ω_i corresponding to the Fourier-chirped-Gaussian profile and the Fourier-Hermite-Gaussian profile.

VI. NUMERICAL IMPLEMENTATION–3D

In this section, we address the complete numerical solution of the initial boundary-value problem (IBVP) stated in (51). The formulation of the discrete linear system for the IBVP requires temporal as well as spatial discretization of the problem. For the computational domain Ω_i , we introduce a reference domain $\Omega_i^{\text{ref}} = \mathbb{I} \times \pi\mathbb{I} \times \pi\mathbb{I}$ keeping in view the typical domain of definition of the orthogonal polynomials being used. In order to describe the associated linear maps between the reference domain and the actual computational domain, we introduce the

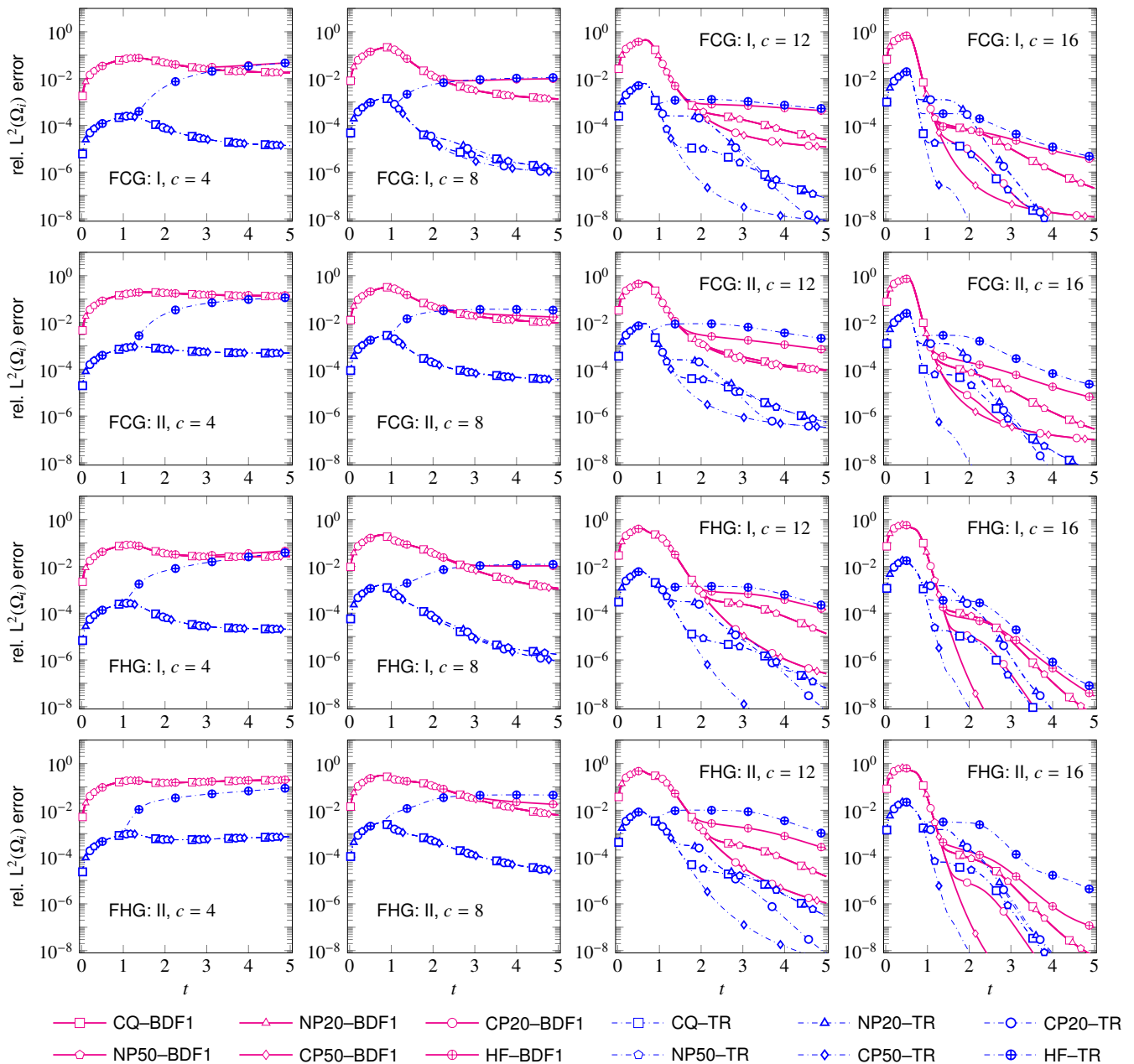


FIG. 7. The figure shows a comparison of evolution of error in the numerical solution of the IBVP (14) with various approximations of the TBCs corresponding to the Fourier-chirped-Gaussian and the Fourier-Hermite-Gaussian profiles with different values of the speed ‘ c ’ (see Table I and Table II). The numerical parameters and the labels are described in Sec. VB where the error is quantified by (169).

variables $y_1, y_2, y_3 \in \Omega_i^{\text{ref}}$ such that

$$\begin{aligned}
 x_1 &= J_1 y_1 + \bar{x}_1, & J_1 &= \frac{1}{2}(x_r - x_l), & \bar{x}_1 &= \frac{1}{2}(x_l + x_r), \\
 x_2 &= J_2 y_2, & J_2 &= \frac{d_2}{\pi}, & \beta_1 &= J_1^{-2}, & \beta_2 &= \beta J_2^{-2}, \\
 x_3 &= J_3 y_3, & J_3 &= \frac{d_3}{\pi}, & \beta_3 &= \beta J_3^{-2},
 \end{aligned}$$

Let Δt denote the time-step. In the rest of the section, with a slight abuse of notation, we switch to the variables $y_1 \in \mathbb{I}$ and $y_2 = y_3 \in \pi\mathbb{I}$ for all the discrete approximations of the dependent variables. For instance, $u^j(\mathbf{y})$ is taken to approximate $u(\mathbf{x}, j\Delta t)$ for $j = 0, 1, 2, \dots, N_t - 1$. The temporal discretization of the interior problem using one-step methods is enumerated below:

TABLE IV. Numerical parameters for studying the convergence error

Computational domain (Ω_i)	$(-10, 10) \times [-\pi, \pi)$
Maximum time (T_{max})	5
Set of no. of time-steps (\mathbb{N}_t)	$\{2^8, 2^9, \dots, 2^{16}\}$
Time-step	$\{\Delta t = T_{max}/(N_t - 1), N_t \in \mathbb{N}_t\}$
Number of LGL-points ($(N + 1) \times (N + 1)$)	200×200

- The BDF1 based discretization is given by

$$i \frac{u^{j+1} - u^j}{\Delta t} + \Delta u^{j+1} = 0, \quad \rho = 1/\Delta t, \quad (171)$$

$$(\beta_1 \partial_{y_1}^2 + \beta_2 \partial_{y_2}^2 + \beta_3 \partial_{y_3}^2) u^{j+1} + i \rho u^{j+1} = i \rho u^j.$$

- The TR based discretization is given by

$$i \frac{u^{j+1} - u^j}{\Delta t} + \Delta u^{j+1/2} = 0, \quad \rho = 2/\Delta t, \quad (172)$$

$$(\beta_1 \partial_{y_1}^2 + \beta_2 \partial_{y_2}^2 + \beta_3 \partial_{y_3}^2) v^{j+1} + i \rho v^{j+1} = i \rho u^j,$$

where we have used the staggered samples of the field in the last step. The rest of this section is organized as follows: Sec. VI A addresses the temporal discretization of the boundary maps which is followed by a discussion of the resulting spatial problem in Sec. VI B.

A. Discretizing the boundary conditions

As discussed above, we aim at a compatible temporal discretization of the novel boundary conditions formulated in Sec. III B in order to solve the IBVP in (51). In order to facilitate the temporal discretization of the TBCs, we introduce the equispaced samples of the auxiliary function, $\varphi^{j,k}(\mathbf{y})$, to approximate $\varphi(\mathbf{x}, j\Delta t, k\Delta t)$ for $j, k = 0, 1, \dots, N_t - 1$. It follows from the definition of the auxiliary function that the diagonal values of the auxiliary function at the discrete level are determined by the interior field, i.e., $\varphi^{j,j}(y_1, y_2, y_3) = u^j(y_1, y_2, y_3)$. For the space discretization of the auxiliary equation on the faces of Ω_i , we use the Fourier-Galerkin method which employs the series

$$\varphi^{j,k}(\mathbf{y}) = \sum_{m_2 \in \mathbb{J}_2} \sum_{m_3 \in \mathbb{J}_3} \tilde{\varphi}_{m_2, m_3}^{j,k}(\mathbf{y}) e^{i(m_2 y_2 + m_3 y_3)}, \quad (173)$$

where the index set is given by

$$\mathbb{J}_p = \left\{ -\frac{N_p}{2}, \dots, \frac{N_p}{2} - 1 \right\}, \quad p = 2, 3. \quad (174)$$

For the sake of brevity of presentation, let $\tilde{\varphi}_{\mathbf{m}}^{j,k}$ represent the Fourier samples of the auxiliary function i.e. $\tilde{\varphi}_{m_2, m_3}^{j,k}$.

1. NP-BDF1

The discrete scheme for the boundary maps is said to be ‘NP-BDF1’ if the temporal derivatives in the realization of the boundary maps, dubbed as ‘NP’, developed in Sec. III B are discretized using the one-step method BDF1. To achieve this, we start by writing the time-discrete form of the DtN maps present in (63) in the reference domain as

$$\sqrt{\beta_1} \partial_{y_1} \tilde{u}_{\mathbf{m}}^{j+1} \pm e^{-i\pi/4} \left[b_0 \tilde{u}_{\mathbf{m}}^{j+1} - \sum_{k=1}^M b_k \tilde{\varphi}_{k, \mathbf{m}}^{j+1, j+1} \right] = 0. \quad (175)$$

In order to turn these equations into a Robin-type boundary condition, we need to compute the discrete samples $\tilde{\varphi}_{k, \mathbf{m}}^{j+1, j+1}$ by considering the ODEs established for these auxiliary function earlier. Here, we discuss the BDF1-based discretization of (62) by first employing Fourier expansion: Setting $\rho = 1/\Delta t$ and for $k = 1, 2, \dots, M$, we have

$$\frac{\tilde{\varphi}_{k, \mathbf{m}}^{j+1, j+1} - \tilde{\varphi}_{k, \mathbf{m}}^{j, j+1}}{\Delta t} + \eta_k^2 \tilde{\varphi}_{k, \mathbf{m}}^{j+1, j+1} = \tilde{\varphi}_{\mathbf{m}}^{j+1, j+1}$$

$$\tilde{\varphi}_{k, \mathbf{m}}^{j+1, j+1} = \frac{\rho}{(\rho + \eta_k^2)} \tilde{\varphi}_{k, \mathbf{m}}^{j, j+1} + \frac{1}{(\rho + \eta_k^2)} \tilde{u}_{\mathbf{m}}^{j+1}. \quad (176)$$

Introduce the scaling $\bar{\eta}_k = \eta_k / \sqrt{\rho}$ so that

$$\tilde{\varphi}_{k, \mathbf{m}}^{j+1, j+1} = \frac{1}{(1 + \bar{\eta}_k^2)} \left[\tilde{\varphi}_{k, \mathbf{m}}^{j, j+1} + \frac{1}{\rho} \tilde{u}_{\mathbf{m}}^{j+1} \right]. \quad (177)$$

The value of $\tilde{\varphi}_{k, \mathbf{m}}^{j, j+1}$ can be obtained by propagation along τ_{\perp} using $\tilde{\varphi}_{k, \mathbf{m}}^{j, j}$ as the initial condition in (55):

$$\tilde{\varphi}_{k, \mathbf{m}}^{j, j+1} = \frac{1}{(1 + \alpha_2^{-2} m_2^2 + \alpha_3^{-2} m_3^2)} \tilde{\varphi}_{k, \mathbf{m}}^{j, j}, \quad (178)$$

where $m_p \in \mathbb{J}_p$, $p = 2, 3$. Next we plug-in the value of the auxiliary field, $\tilde{\varphi}_{k, \mathbf{m}}^{j+1, j+1}$, in (175) to obtain

$$\partial_{y_1} \tilde{u}_{\mathbf{m}}^{j+1} \pm \alpha_1 \varpi \tilde{u}_{\mathbf{m}}^{j+1}$$

$$= \mp \frac{\alpha_1}{(1 + \alpha_2^{-2} m_2^2 + \alpha_3^{-2} m_3^2)} \left[\sum_{k=1}^M \Gamma_k \tilde{\varphi}_{k, \mathbf{m}}^{j, j} \right]$$

$$= \mp \alpha_1 \tilde{\mathcal{B}}_{\mathbf{m}, \alpha_1}^{j+1}, \quad (179)$$

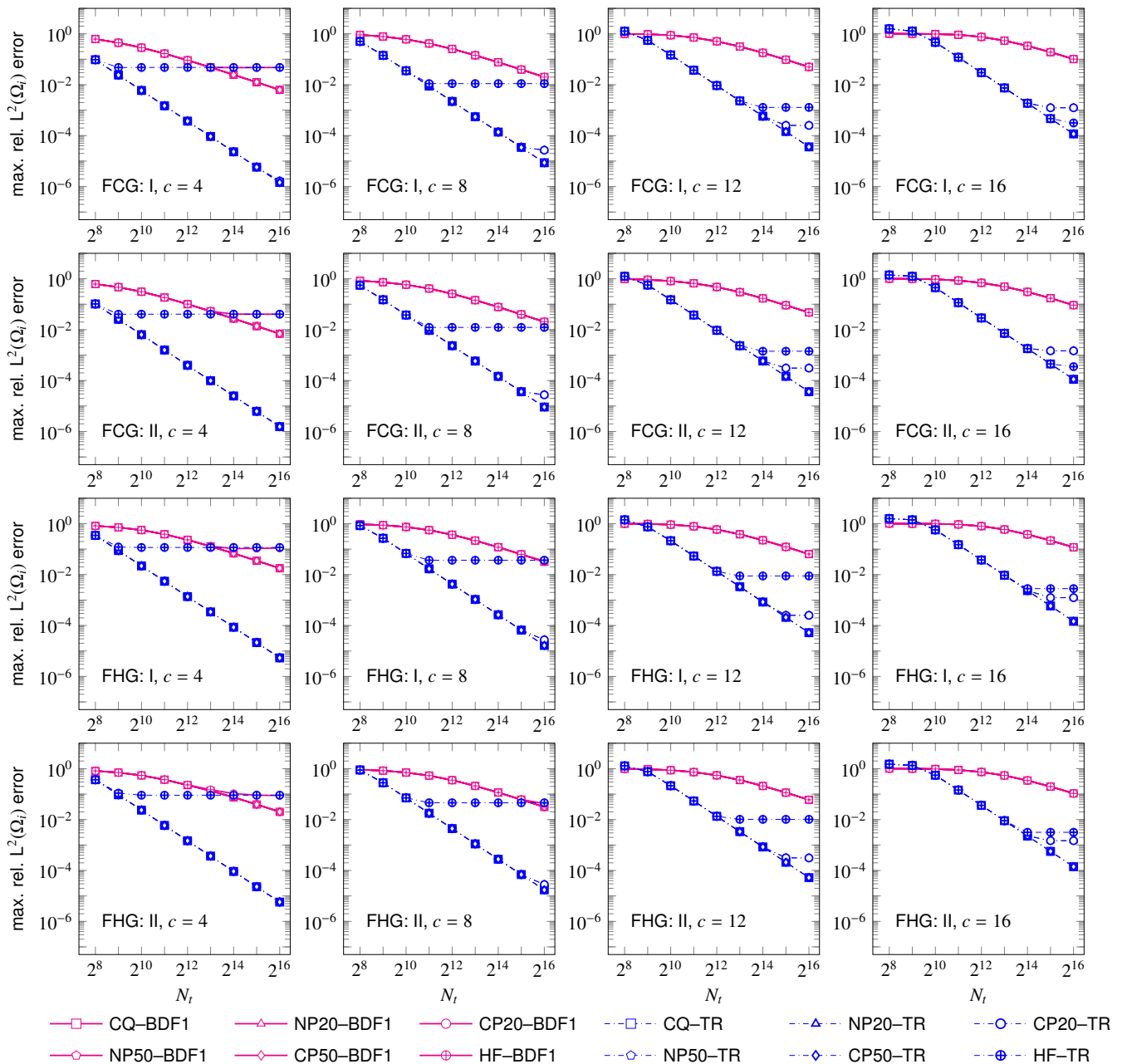


FIG. 8. The figure depicts the convergence behaviour of the numerical solution of the IBVP (14) with various approximations of the TBCs corresponding to the Fourier-chirped-Gaussian and the Fourier-Hermite-Gaussian profiles with different values of the speed ‘c’ (see Table I and Table II). The numerical parameters and the labels are described in Sec. VC where the error is quantified by (170).

where we have set $\bar{b}_0 = b_0/\sqrt{\rho}$, $\bar{b}_k = b_k/\sqrt{\rho}$ and

$$\varpi = \bar{b}_0 + \frac{1}{\rho} \sum_{k=1}^M \Gamma_k, \quad \Gamma_k = -\bar{b}_k/(1 + \bar{\eta}_k^2). \quad (180)$$

Note that these Robin type maps are written for each component in the Fourier expansion.

2. NP-TR

The discrete scheme for the boundary maps is said to be ‘NP-TR’ if the temporal derivatives in the realization of the boundary maps, dubbed as ‘NP’, developed in Sec. IIIB are discretized using the one-step method TR. To achieve this, we start by writing the time-discrete form of the DtN maps present in (63) in the reference do-

main as

$$\sqrt{\beta_1} \partial_{y_1} \tilde{v}_m^{j+1} \pm e^{-i\pi/4} \left[b_0 \tilde{v}_m^{j+1} - \sum_{k=1}^M b_k \tilde{\varphi}_{k,m}^{j+1/2,j+1/2} \right] = 0. \quad (181)$$

In order to turn these equations into a Robin-type boundary condition, we need to compute the discrete samples $\varphi_{k,m}^{j+1/2,j+1/2}$ by considering the ODEs established for these auxiliary function earlier. Here, we discuss the TR-based discretization of (62) by first employing Fourier expansion: Setting $\rho = 2/\Delta t$ and for $k = 1, 2, \dots, M$, we have

$$\frac{\tilde{\varphi}_{k,m}^{j+1,j+1} - \tilde{\varphi}_{k,m}^{j,j+1}}{\Delta t} + \eta_k^2 \frac{\tilde{\varphi}_{k,m}^{j+1,j+1} + \tilde{\varphi}_{k,m}^{j,j+1}}{2} = \frac{\tilde{\varphi}_m^{j+1,j+1} + \tilde{\varphi}_m^{j,j+1}}{2}. \quad (182)$$

Introduce the scaling $\bar{\eta}_k = \eta_k/\sqrt{\rho}$ so that

$$\tilde{\varphi}_{k,m}^{j+1,j+1} = \frac{(1 - \bar{\eta}_k^2)}{(1 + \bar{\eta}_k^2)} \tilde{\varphi}_{k,m}^{j,j+1} + \frac{2/\rho}{(1 + \bar{\eta}_k^2)} \left[\tilde{v}_m^{j+1} + \frac{\tilde{\varphi}_m^{j,j+1} - \tilde{\varphi}_m^{j,j}}{2} \right]. \quad (183)$$

For the staggered configuration, we have

$$\tilde{\varphi}_{k,m}^{j+1/2,j+1/2} = \frac{1}{2} \left[\left(\frac{1 - \bar{\eta}_k^2}{1 + \bar{\eta}_k^2} \right) \tilde{\varphi}_{k,m}^{j,j+1} + \tilde{\varphi}_{k,m}^{j,j} \right] + \frac{1/\rho}{(1 + \bar{\eta}_k^2)} \left[\tilde{v}_m^{j+1} + \frac{\tilde{\varphi}_m^{j,j+1} - \tilde{\varphi}_m^{j,j}}{2} \right]. \quad (184)$$

The values of $\tilde{\varphi}_{k,m}^{j,j+1}$ and $\tilde{\varphi}_m^{j,j+1}$ can be obtained by propagation along τ_\perp using $\tilde{\varphi}_{k,m}^{j,j}$ and $\tilde{\varphi}_m^{j,j}$ as the initial condition:

$$\tilde{\varphi}_{k,m}^{j,j+1} = \frac{(1 - \alpha_2^{-2} m_2^2 - \alpha_3^{-2} m_3^2)}{(1 + \alpha_2^{-2} m_2^2 + \alpha_3^{-2} m_3^2)} \tilde{\varphi}_{k,m}^{j,j},$$

$$\frac{1}{2} [\tilde{\varphi}_m^{j,j+1} - \tilde{\varphi}_m^{j,j}] = \frac{(-\alpha_2^{-2} m_2^2 - \alpha_3^{-2} m_3^2)}{(1 + \alpha_2^{-2} m_2^2 + \alpha_3^{-2} m_3^2)} \tilde{\varphi}_m^{j,j}. \quad (185)$$

Next we plug-in the value of $\tilde{\varphi}_{k,m}^{j+1/2,j+1/2}$ in (181) which leads to following compact form of the boundary maps

$$\partial_{y_1} \tilde{v}_m^{j+1} \pm \alpha_1 \varpi \tilde{v}_m^{j+1} = \mp \alpha_1 \tilde{\mathcal{B}}_{m,a_1}^{j+1/2}, \quad (186)$$

where ϖ is same as that in BDF1 and the history functions are given by

$$\tilde{\mathcal{B}}_{m,a_1}^{j+1/2} = \sum_{k=1}^M \frac{-\bar{b}_k}{2} \tilde{\varphi}_{k,m}^{j,j} + \sum_{k=1}^M \frac{\Gamma_k}{\rho} \left(\frac{-\alpha_2^{-2} m_2^2 - \alpha_3^{-2} m_3^2}{1 + \alpha_2^{-2} m_2^2 + \alpha_3^{-2} m_3^2} \right) \tilde{u}_m^j + \sum_{k=1}^M \frac{-\bar{b}_k}{2} \left(\frac{1 - \bar{\eta}_k^2}{1 + \bar{\eta}_k^2} \right) \left(\frac{1 - \alpha_2^{-2} m_2^2 - \alpha_3^{-2} m_3^2}{1 + \alpha_2^{-2} m_2^2 + \alpha_3^{-2} m_3^2} \right) \tilde{\varphi}_{k,m}^{j,j} \quad (187)$$

Note that these Robin type maps are written for each component in Fourier expansion.

B. Numerical Solution of the IBVP

Having discussed the temporal discretization of the 3D problem, we now aim at the spatial discretization using Legendre Galerkin spectral method. Recall the form of the TBCs (for NP methods) casted as Robin-type boundary maps specific to each Fourier component:

$$\partial_{y_1} \tilde{u}_m^{j+1} \pm \alpha_1 \varpi \tilde{u}_m^{j+1} = \mp \alpha_1 \tilde{\mathcal{B}}_{m,a_1}^{j+1}, \quad a_1 \in \{r, l\}. \quad (188)$$

Following along the similar lines as discussed for the case of 2D problem, we define the space of boundary-adapted basis to enforce these maps exactly as

$$\mathcal{W}_N = \left\{ \tilde{u}_m \in \mathcal{P}_N \mid \begin{aligned} (\partial_{y_1} - \kappa) \tilde{u}_m(y_1) \Big|_{y_1=-1} &= 0, \\ (\partial_{y_1} + \kappa) \tilde{u}_m(y_1) \Big|_{y_1=+1} &= 0 \end{aligned} \right\},$$

where $\kappa = \alpha_1 \varpi$ which is determined by the Robin-type formulation of the TBCs for NP methods. We introduce a function χ_m to convert the discrete BCs to a homogeneous form by stating the original field as $\tilde{u}_m^j = \tilde{w}_m^j + \chi_m^j(y_1)$ where $\tilde{w}_m^j \in \mathcal{W}_N$ so that

$$\begin{aligned} [-\alpha_1^{-2} \partial_{y_1}^2 + \alpha_2^{-2} m_2^2 + \alpha_3^{-2} m_3^2 + 1] (\tilde{w}_m^{j+1} + \chi_m^{j+1}) &= \tilde{w}_m^j, \\ (\partial_{y_1} - \kappa) \tilde{w}_m^{j+1} \Big|_{y_1=-1} &= 0, \\ (\partial_{y_1} + \kappa) \tilde{w}_m^{j+1} \Big|_{y_1=+1} &= 0, \end{aligned}$$

and the field $\chi_m^j(y_1)$ is forced to satisfy the constraints:

$$\begin{aligned} (\partial_{y_1} - \kappa) \chi_m^j(y_1) \Big|_{y_1=-1} &= +\alpha_1 \tilde{\mathcal{B}}_{m,l}^j, \\ (\partial_{y_1} + \kappa) \chi_m^j(y_1) \Big|_{y_1=+1} &= -\alpha_1 \tilde{\mathcal{B}}_{m,r}^j, \end{aligned} \quad (189)$$

Following in the similar manner as in 2D case, the lifting functions for this case works out to be

$$\begin{cases} \chi_l(y_1) = -\frac{1}{2\kappa} L_0(y_1) + \frac{1}{2(\kappa+1)} L_1(y_1), \\ \chi_r(y_1) = +\frac{1}{2\kappa} L_0(y_1) + \frac{1}{2(\kappa+1)} L_1(y_1). \end{cases} \quad (190)$$

The lifted field becomes

$$\tilde{u}_m^j(y_1) = \tilde{w}_m^j(y_1) + \alpha_1 \chi_l \tilde{\mathcal{B}}_{m,l}^j - \alpha_1 \chi_r \tilde{\mathcal{B}}_{m,r}^j, \quad (191)$$

Next, we choose the basis $\theta_p \in \mathcal{W}_N$ defined as

$$\theta_p(y_1) = \phi_p(y_1), \quad p \in \mathbb{J}_1, \quad (192)$$

where $\{\phi_p \mid p \in \mathbb{J}_1\}$ can be constructed using the ansatz $\phi_p(y_1) = L_p(y_1) + a_p L_{p+1}(y_1) + b_p L_{p+2}(y_1)$. Imposing the boundary conditions in the definition of \mathcal{W}_N , the sequences $(a_p)_{p \in \mathbb{J}_1}$ and $(b_p)_{p \in \mathbb{J}_1}$ work out to be

$$a_p = 0, \quad b_p = -\frac{\kappa + \frac{1}{2}p(p+1)}{\kappa + \frac{1}{2}(p+2)(p+3)}, \quad p \in \mathbb{J}_1. \quad (193)$$

TABLE V. Numerical parameters for studying the evolution error

Computational domain (Ω_i)	$(-10, 10) \times [-\pi, \pi] \times [-\pi, \pi]$
Maximum time (T_{max})	5
No. of time-steps (N_t)	5000 + 1
Time-step (Δt)	$10^{-3} = T_{max}/(N_t - 1)$
Number of LGL-points ($(N + 1) \times (N + 1) \times (N + 1)$)	$100 \times 100 \times 100$

The mass and stiffness matrices with the boundary-adapted basis functions remain same as described for NP method (in 2D problem) due to the fact that ϖ present in TBCs is independent of the Fourier component. The variational formulation then works out to be

$$-\alpha_1^{-2} (\partial_{y_1}^2 \tilde{w}_{\mathbf{m}}^{j+1}, \theta_p) + [1 + \alpha_2^{-2} m_2^2 + \alpha_3^{-2} m_3^2] (\tilde{w}_{\mathbf{m}}^{j+1}, \theta_p) = (\tilde{u}_{\mathbf{m}}^j, \theta_p) + \mathcal{I} \quad (194)$$

where

$$\mathcal{I} = \alpha_1 \mathcal{D}_{\mathbf{m}} \left[(\tilde{\mathcal{B}}_{\mathbf{m},r}^{j+1} \chi_r, \theta_p) - (\tilde{\mathcal{B}}_{\mathbf{m},l}^{j+1} \chi_l, \theta_p) \right]. \quad (195)$$

and $\mathcal{D}_{\mathbf{m}} = (1 + \alpha_2^{-2} m_2^2 + \alpha_3^{-2} m_3^2)$. To further simplify the terms on right hand side, let $\tilde{f}_{\mathbf{m}}^j$ be such that

$$\mathcal{D}_{\mathbf{m}} [\alpha_1 \tilde{\mathcal{B}}_{\mathbf{m},r}^{j+1} \tilde{\chi}_r(y_1) - \alpha_1 \tilde{\mathcal{B}}_{\mathbf{m},l}^{j+1} \tilde{\chi}_l(y_1)] + \tilde{u}_{\mathbf{m}}^j = \tilde{f}_{\mathbf{m}}^j, \quad (196)$$

then it follows that

$$\tilde{f}_{\mathbf{m}}^j = \tilde{u}_{\mathbf{m}}^j + \frac{\alpha_1 \mathcal{D}_{\mathbf{m}}}{2\kappa} \left[\tilde{\mathcal{B}}_{\mathbf{m},r}^{j+1} + \tilde{\mathcal{B}}_{\mathbf{m},l}^{j+1} \right] L_0(y_1) + \frac{\alpha_1 \mathcal{D}_{\mathbf{m}}}{2(1+\kappa)} \left[\tilde{\mathcal{B}}_{\mathbf{m},r}^{j+1} - \tilde{\mathcal{B}}_{\mathbf{m},l}^{j+1} \right] L_1(y_1). \quad (197)$$

Let $\tilde{u}_{p,\mathbf{m}}$ denote the expansion coefficients of the field $\tilde{u}_{\mathbf{m}}$ in Legendre basis for each \mathbf{m} -th Fourier component and $\tilde{w}_{p,\mathbf{m}}$ denote the expansion coefficients in the boundary-adapted basis as

$$\begin{aligned} \tilde{w}_{\mathbf{m}}^{j+1} &= \sum_{p \in \mathbb{J}_1} \tilde{w}_{p,\mathbf{m}}^{j+1} \theta_p(y_1) = \sum_{p' \in \mathbb{J}_1} \tilde{w}_{p',\mathbf{m}}^{j+1} \phi_{p'}(y_1), \\ \tilde{u}_{\mathbf{m}}^j &= \sum_{p=0}^N \tilde{u}_{p,\mathbf{m}}^{j+1} L_p(y_1). \end{aligned} \quad (198)$$

The inner product $(\tilde{f}_{\mathbf{m}}^j, \theta_p)$ can be computed from the knowledge of the Legendre coefficients of the field $\tilde{f}_{\mathbf{m}}^j$ using the specific form of the boundary-adapted basis. This can be achieved via *quadrature matrix* given in A. The linear system thus becomes

$$[\alpha_1^{-2} S_1 + \mathcal{D}_{\mathbf{m}} M_1] \hat{\mathbf{w}}_{\mathbf{m}}^{j+1} = Q_1 \Gamma \tilde{\mathbf{f}}_{\mathbf{m}}^j.$$

The mass and stiffness matrices are defined in (131) and the linear system is then solved using LU-decomposition method.

VII. NUMERICAL EXPERIMENTS-3D

In this section, we will carry out some numerical tests to showcase the accuracy of the numerical schemes developed in this work to solve the IBVP (51), focusing on the case $\beta = +1$. We start by writing the exact solutions for the IBVP under consideration followed by studying the error evolution behaviour of the numerical schemes.

A. Fourier-Chirped-Gaussian profile

For the 3D problem, we restrict ourselves to the Fourier-chirped-Gaussian profiles for the choice of exact solutions. Recalling the function \mathcal{G} from Sec. VA, we can define a family of solutions (for the 3D problem) referred to as Fourier-chirped-Gaussian profile given by

$$G(\mathbf{x}, t; a, b, c, \zeta_{\perp}) = \mathcal{G}(x_1 - c_1 t, t; a, b) \exp\left(+i\frac{1}{2} c x_1 - i\frac{1}{4} c^2 t\right) \exp(i\zeta_{\perp} \cdot \mathbf{x}_{\perp} - i\zeta_{\perp}^2 t), \quad (199)$$

where ζ_{\perp} denote the covariable corresponding to \mathbf{x}_{\perp} used in the two dimensional Fourier transform. Rest of the parameters are same as described in Sec. VA. The specific values of the parameters of the solutions used in the numerical experiments are summarized in Table I assuming $\zeta_2 = \zeta_3 = \zeta$ which means we take the periodicity to be same along \mathbf{e}_2 and \mathbf{e}_3 . The profiles are chosen with non-zero speed c_0 so that the field hits the boundary of Ω_i .

B. Tests for evolution error

In this section, we consider the IBVP in (51) where the initial condition corresponds to the exact solutions described in Sec. VII A. The error in the evolution of the profile computed numerically is quantified by the relative $L^2(\Omega_i)$ -norm defined in Sec. VB.

For the 3D problem, we only consider the novel-Padé based discrete versions of the DtN maps, namely, NP. They have a variant determined by the choice of one-step method used in the temporal discretization so that the complete list of methods to be tested can be labelled as NP-BDF1, (corresponding to the one-step method

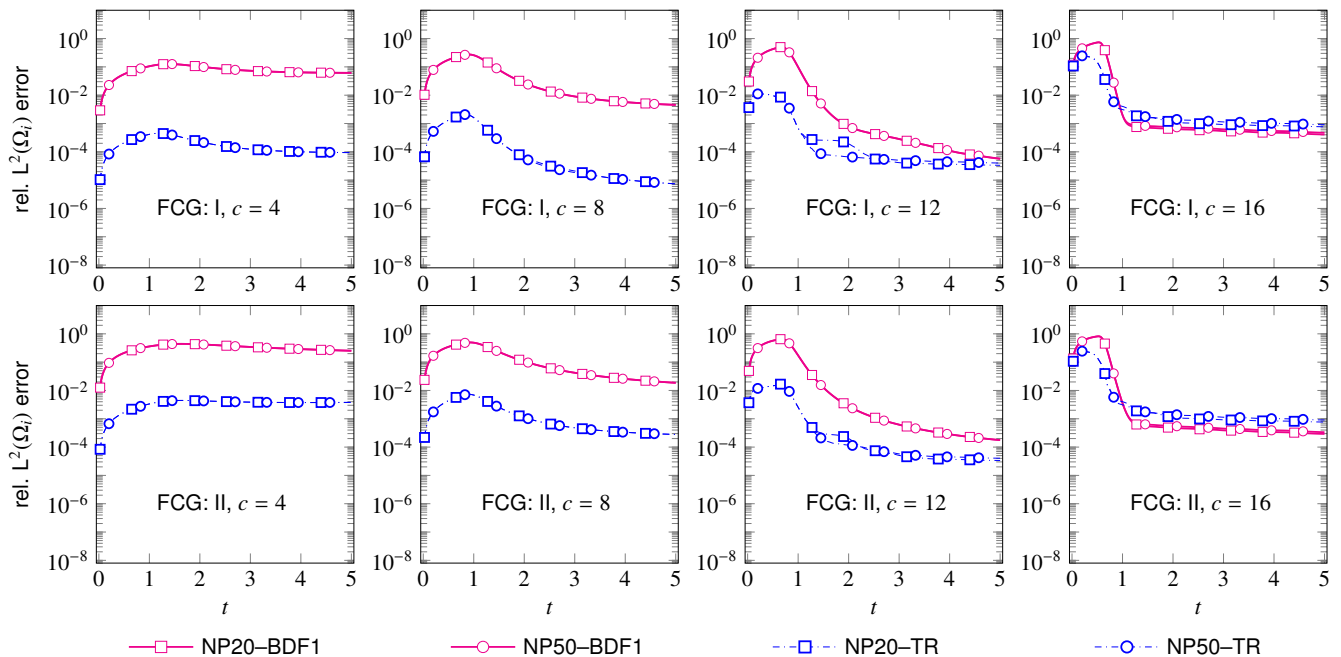


FIG. 9. The figure shows a comparison of evolution of error in the numerical solution of the IBVP (51) with novel Padé based approximation of the TBCs corresponding to the Fourier-chirped-Gaussian profile with different values of the speed ‘ c ’ (see Table I). The numerical parameters and the labels are described in Sec. VII B where the error is quantified by (169).

BDF1), and, NP-TR (corresponding to the one-step method TR). For the Padé approximant based method (NP), we distinguish the diagonal approximant of order 20 from that of 50 via the labels ‘NP20’ and ‘NP50’. The numerical parameters used in this section are summarized in Table V. The exact solutions used are defined in Sec. VII A.

The numerical results for the evolution error on Ω_i corresponding to the Fourier-chirped-Gaussian profile are shown in Fig. 9. It can be seen that the diagonal Padé approximants based method, namely, NP, show stable behaviour. Observe that the TR methods perform better than the BDF1 methods which is clear from the error peaks in Fig. 9. Note that the accuracy deteriorates with increase in the value of c which can be seen from the error peaks in the Fig. 9. This behaviour can be attributed to the increased oscillatory nature of the solution. Moreover, for the faster moving profiles, error curves plateaus after certain number of time steps.

VIII. CONCLUSION

In this work, we presented an efficient numerical implementation of the transparent boundary operator and its various approximations for the case of free Schrödinger equation on a rectangular computational domain with periodicity assumption along a subset of the unbounded directions. More specifically, we compared the performance of various approximations of the transpar-

ent boundary operator, namely, convolution quadrature based approach, conventional Padé approach, novel Padé approach and high-frequency approximation method. Next, keeping in mind the superior accuracy and lower computational complexity of novel Padé method (in comparison to rest of the approaches), we extend the novel Padé approach for the TBCs corresponding to free Schrödinger equation on a hyperrectangular computational domain in 3D.

For the spatial problem, we use a Legendre-Fourier Galerkin method where a boundary adapted basis is constructed using Legendre polynomials that ensures the bandedness of the resulting linear system. Temporal discretization is addressed with two one-step methods, namely BDF1 and TR. As far as time-marching is concerned, we would like to mention that any higher order one-step method can be readily used with the novel Padé method to further enhance the accuracy of the numerical schemes. Several numerical tests are carried out to demonstrate the efficiency and empirical stability of various numerical schemes for the 2D as well as the 3D problem under consideration. Theoretical proofs for stability and convergence of our numerical schemes are beyond the scope of this paper. We defer these issues to a future publication. Extension of the ideas presented in this paper to more general systems will be explored in future publications.

